processes

MDPI

Article

A Study on Large Electric Vehicle Fires in a Tunnel: Use of a Fire Dynamics Simulator (FDS)

Roberto Dessì [1], Daniel Fruhwirt [2] and Davide Papurello [1,3,*]

[1] Department of Energy, Politecnico di Torino, Corso Duca degli Abruzzi, 24, 10129 Turin, Italy
[2] Institute of Thermodynamics and Sustainable Propulsion Systems, Graz University of Technology, Inffeldgasse 25D, 8010 Graz, Austria
[3] Energy Center, Politecnico di Torino, Via P. Borsellino 38/18, 10138 Turin, Italy
* Correspondence: davide.papurello@polito.it

Abstract

Internal combustion engine vehicles damage the environment and public health by emitting toxic fumes, such as CO_2 or CO and other trace compounds. The use of electric cars helps to reduce the emission of pollutants into the environment due to the use of batteries with no direct and local emissions. However, accidents of battery electric vehicles pose new challenges, such as thermal runaway. Such accidents can be serious and, in some cases, may result in uncontrolled overheating that causes the battery pack to spontaneously ignite. In particular, the most dangerous vehicles are heavy goods vehicles (HGVs), as they release a large amount of energy that generate high temperatures, poor visibility, and respiratory damage. This study aims to determine the potential consequences of large BEV fires in road tunnels using computational fluid dynamics (CFD). Furthermore, a comparison between a BEV and an ICEV fire shows the differences related to the thermal and the toxic impact. Furthermore, the adoption of a longitudinal ventilation system in the tunnel helped to mitigate the BEV fire risk, keeping a safer environment for tunnel users and rescue services through adequate smoke control.

Keywords: electric vehicle; thermal runaway; road tunnels; fires; fire dynamics simulator; heat release rate; impulse ventilation

Academic Editor: Albert Ratner

Received: 1 July 2025
Revised: 28 July 2025
Accepted: 29 July 2025
Published: 31 July 2025

Citation: Dessì, R.; Fruhwirt, D.; Papurello, D. A Study on Large Electric Vehicle Fires in a Tunnel: Use of a Fire Dynamics Simulator (FDS). *Processes* **2025**, *13*, 2435. https://doi.org/10.3390/pr13082435

1. Introduction

The automotive industry has played a leading role in both global economic development and the pursuit of new technologies [1]. The use of vehicles to reach distant destinations quickly and safely is a crucial asset for a country's growth. However, the use of fossil fuels leads to the emission of substances harmful to the environment and human health, such as sulphur dioxide (SO_2), nitrogen oxides (NO_x), carbon monoxide (CO), and particulate matter (PM). On a global scale, 26% of primary energy is consumed by the transport sector, which accounts for about 23% of greenhouse gas (GHG) emissions [2]. Saleh [3] conducted a study on 27 EU countries regarding transportation pollution and found that carbon-derived substances from vehicles accounted for 25% of total CO_2 emissions. Over nearly 30 years, GHG production in domestic transport has increased by almost 30% compared to the residential and commercial sectors. To avoid pollution problems and to cut dependence on petroleum derivatives, the concept of "sustainable transport" has emerged, promoted through using electric vehicles (EVs) coupled with green energy production. EVs offer numerous advantages, including reduced emissions, low operating costs, clean energy

sources, high WTW efficiency, low noise, maximum convenience, and instant maximum torque from the start. Politically, the main argument for replacing conventional vehicles with BEVs is the reduction of GHG emissions, although the total cost of ownership is decisive, especially in the commercial sector. According to the IEA Global Outlook 2024 report [4], nearly 14 million new vehicles were registered globally in 2023, bringing the total number of EVs on the roads to 40 million. A significant data point is the increase in sales of larger vehicles, which are a greater source of pollution compared to cars. The electrification of buses, heavy-duty trucks (HD trucks), medium-duty trucks (MD trucks), and special vehicles has increased to avoid negative effects on the global climate. The IEA report also showed a significant reduction for the CO_2 equivalent produced by the batteries of BEVs and PHEVs, compared to those of internal combustion engine vehicles. Thanks to the decarbonisation of power generation, it is estimated that, by 2035, the lifecycle emissions intensity of a BEV battery could reach a maximum of 18%, highlighting the priority of research in solving the climate change problem. Another key aspect is the safety that vehicles must guarantee if thermal runaway and uncontrolled heating leading to spontaneous ignition. In particular, thermal runaway is the main cause of fires in vehicles equipped with lithium-ion batteries, as phenomena such as overcharging, exceeding a critical temperature threshold, and cell damage can lead to fires and other hazardous events. Sun et al. [5] highlighted that 13% of fires in parked vehicles are related to extreme temperature variations between day and night. Their study also emphasised that 26% of the fires occurring during charging sessions are due to overcharging, direct battery ignition, or malfunctions in the charging equipment. Due to new regulations aimed at reducing the number of pollutants in exhaust gases released by vehicle tailpipes, extensive research is being conducted into the causes and consequences of fires to understand fire risks. In Australia, 90% of tunnel fires are caused by vehicle structural defects and 10% by collisions [6]. To prevent fire from spreading further and causing more damage, water-based extinguishing systems and mechanical ventilation systems are used to mitigate the consequences of fires. Bai et al. [7] conducted an analysis of 156 fires in tunnels in China and discovered that they are more frequent in economically developed areas. Furthermore, their study highlighted a high probability of fires caused by heavy traffic (35.9%) or spontaneous combustion (54.5%) due to factors primarily related to the structural defects in tyres (41.2%) or the engine (41.2%) and occurring at the entrance or exit of long tunnels (up to 200 m from the tunnel portals). EV fires in tunnels are less frequent because these vehicles are still less often used than conventional vehicles (diesel or gasoline) and the BEV fleet is quite new compared to the ICEV fleet. To assess the consequences of large BEV fires, numerical methods of computational fluid dynamics (CFD) are used to reproduce the environmental conditions during a vehicle fire in a confined space, such as a car park or a tunnel, where the danger of evacuation of people and structural instability are greater. Li et al. [8] conducted a study on thermal runaway in lithium-ion batteries. By adjusting the mesh size (more coarse or fine), they obtained a sufficient number of cells to achieve a difference of less than 0.3% between the simulation results and the experimental data, highlighting the high level of accuracy the model can provide. Moreover, with optimal cell division, the abnormal temperature rise caused by the phenomenon was uniform throughout the battery, with differences between cells of only 1 K. The need for experimental data to validate such models and CFD studies, however, is still an open point. The objective of this study is to assess the risks associated with a fire of a large EV inside a tunnel through FDS 6.9.1 and PyroSim software 2024.2, studying various parameters, such as temperature and smoke concentration (reduction of visibility). In the simulation, a ventilation system was also implemented to build up on a realistic and widely used setup. Among the various possible strategies, a longitudinal ventilation system was chosen, capable of pushing the smoke towards the outlet. This

choice, made following EU Directive 2004/54/EC [9,10], is linked to geometric factors (Length < 3 km and traffic volume). To assess the effectiveness of the ventilation system in case of a large EV fire, simulation results with and without the ventilation system were compared. The work is not intended to be quantitative, but a qualitative study of validity related to a comparative approach between fossil-fuelled vehicles and EVs.

2. Materials and Methods

2.1. Pyrosim and FDS

The fire scenario simulation was carried out using PyroSim software from Thunderhead Engineering Consultant. This preprocessor generates the input file needed for the Fire Dynamics Simulator (FDS) to analyse the phenomenon within confined spaces. The FDS is a large-eddy simulation (LES) code for low-speed flows, with an emphasis on smoke and heat transport from fires [11]. The model numerically solves a form of the Navier–Stokes equations. The partial derivatives of the mass, momentum, and energy conservation equations are approximated using finite differences, and the solution is updated over time on a three-dimensional rectilinear grid. Thermal radiation is computed using a finite volume technique on the same grid as the flow solver. Lagrangian particles are used to simulate smoke movement and sprinkler discharge. The software uses a high-definition language (Fortran 90) to solve the equations describing the fire-related phenomena [12]. Every timestep, the software assigns a numerical value to variables, such as temperature, density, pressure, velocity, and chemical composition, for each cell until a defined simulation end time is reached. Furthermore, it calculates quantities that better characterise the fire scenario, such as the mass loss of the vehicle, heat flux, or surface temperature. The classical equations for Newtonian fluids adopted by the FDS are as follows:

- Conservation of mass

$$\frac{\partial \rho}{\partial t} + \nabla \cdot \rho u = \dot{m}_b''' \tag{1}$$

where ρ denotes density [in g/cm^3], t denotes time [in s], u denotes velocity [in m/s], and $\dot{m}_b'''$ represents the net heat flux derived from radiation and thermal conduction phenomena [in kg/s/m^3].

- Conservation of Momentum (Newton's Second Law)

$$\frac{\partial}{\partial t}(\rho u) + \nabla \cdot \rho u u + \nabla p = \rho g + f_b + \nabla \cdot \tau_{ij} \tag{2}$$

where p represents pressure [in Pa], g denotes gravitational acceleration [in m/s^2], f_b denotes the external force applied [in N], and τ_{ij} represents the stress tensor [in N/m^2].

- Conservation of Energy (First Law of Thermodynamics)

$$\frac{\partial}{\partial t}(\rho h) + \nabla \cdot \rho h u = \frac{Dp}{Dt} + \dot{q}''' - \dot{q}_b''' + \nabla \cdot \dot{q}'' + \varepsilon \tag{3}$$

where h represents enthalpy [in J/kg], $\dot{q}'''$ denotes the heat released per unit volume [in W/m^3], $\dot{q}_b'''$ represents the energy transferred to the evaporating droplets [in W/m^3], $\dot{q}''$ indicates the heat flux [in W/m^2], and ε represents the dissipative function [in W/m^3], which is the rate at which kinetic energy is converted into thermal energy due to the viscosity of the fluid (air). To solve the equations mentioned above, the VLES (Very Large Eddy Simulation) was chosen in PyroSim, a mathematical model for simulating turbulence effects. Unlike other models, the VLES is considered an excellent compromise between accuracy and computational cost, as it only analyses large fluid flow rates. Small

fluctuations or vortices are indirectly inferred through the energy spectrum resulting from the large-scale simulation.

2.2. Tunnel Geometry

The shape of the analysed tunnel is based on that of the Rimazzano Tunnel, located on the A12 Livorno–Rosignano Marittimo route of the Trans-European Road network (TEN-T) [13]. The tunnel length measures 920 m (characteristic of the stretch towards Livorno). The tunnel analysed is part of a twin tube tunnel. The tunnel under investigation has two lanes: one for driving and one for overtaking, both 4.05 m wide, flanked by a 0.7 m wide pavement. The tunnel's circumference is 31.42 m. The tunnel geometry was created using the 3D software Autodesk Revit [14]. The project of the Rimazzano Tunnel (a) and the tunnel created with the software (b) are shown in Figure 1.

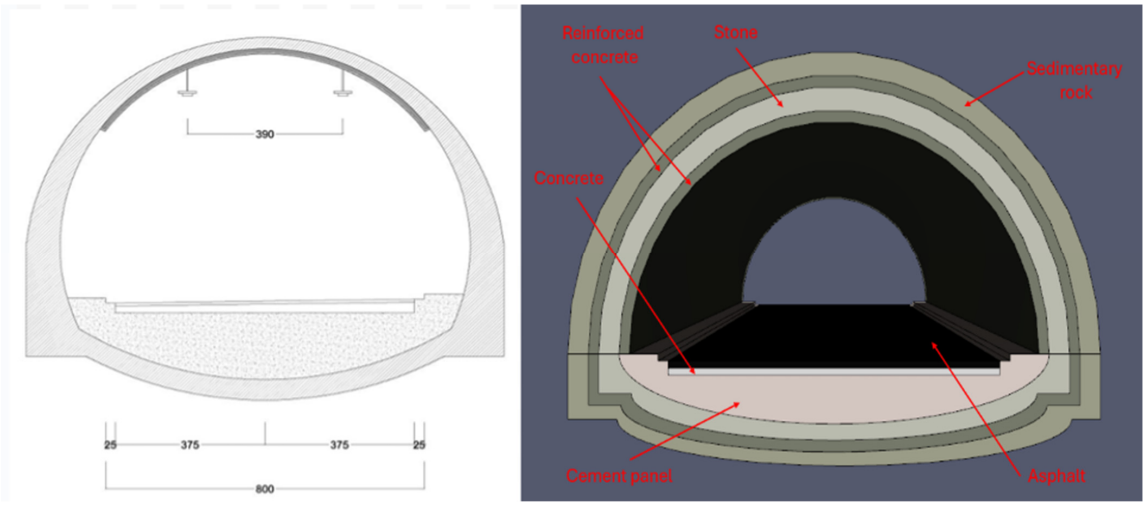

(**a**) (**b**)

Figure 1. (**a**) Rimazzano Tunnel project (on the left). (**b**) mage of the case study created with Revit (on the right).

In Figure 1, the layers composing the tunnel are also shown. Their inclusion is necessary to ensure greater consistency with reality. The following materials are used for the Tunnel project: asphalt, as the layer upon which the cars rest in the tunnel; concrete, as a layer used to provide strength, insulation, and versatility to the structure; reinforced concrete, as a layer resistant to infiltration, wear, and fire; stone, as construction material for the tunnel; cement panel, as a prefabricated cement and reinforced fibre layer, ensuring greater impact resistance and water impermeability; sedimentary rock, as an outer layer that forms the mountains in which the tunnel is excavated. The 3D view of the tunnel created in PyroSim is shown in Figure 2.

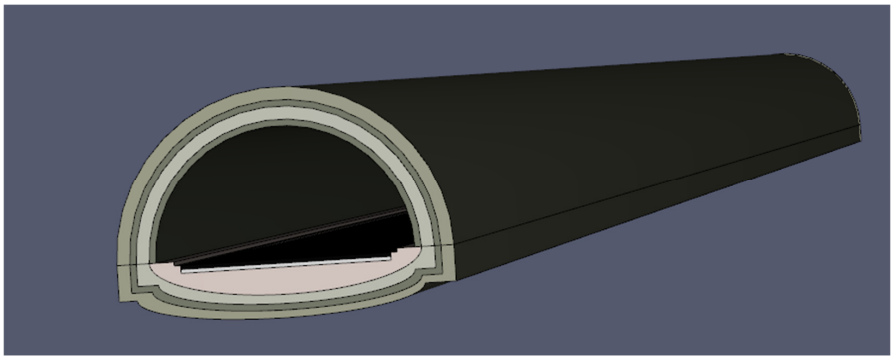

Figure 2. Three-dimensional view of the tunnel in PyroSim.

The thermophysical properties of the materials used for simulation (density, thermal conductivity, specific heat, and emissivity) are listed in Table 1 [15–17].

Table 1. Thermophysical properties of the materials of the constructed tunnel.

Materials	Density ρ [kg/m^3]	Thermal Conductivity k [W/mK]	Specific Heat C_p [kJ/kg·K]	Emissivity ε [-]
Stone	2400	2.4	0.95	0.93
Reinforced concrete	2400	1.6	0.653	0.94
Concrete	2280	1.8	1.04	0.9
Asphalt	2100	0.756	1.67	0.98
Cement panel	2000	1.4	0.78	0.54
Sedimentary rock	2000	1.75	0.95	0.92

2.3. Vehicles

The large vehicle analysed is the SCANIA 25 P BEV, (Scania AB, Södertälje, Sweden) a 100% electric truck in the market since 2022, with a length of 9.965 m, a width of 2.55 m, and a height of 3.109 m [18]. It is equipped with 9 lithium-ion propulsion batteries of 50 Ah, forming a battery pack with a total installed capacity of 300 kWh. It is a 100% EV with a permanent magnet synchronous motor to ensure an extremely stable and precise rotational speed. The actual image (a) and the vehicle representation on PyroSim (b) are shown in Figure 3 (qualitative approach).

(**a**) (**b**)

Figure 3. (**a**) Image of the SCANIA 25 P BEV; (**b**) its representation in PyroSim.

The conventional vehicle is the IVECO Stralis AS 260, a EURO 3 diesel truck (with dimensions and weight similar to the SCANIA) (IVECO (Industrial Vehicles Corporation), Turin, Italy) marketed from 2007 to 2019 [19]. The ICEV is assumed to run on a B7 diesel blend with a 7% RME drop-in, representative for European conditions [ACEA, 2013]. The truck is 9.848 m long, 2.55 m wide, and 3.731 m high. It is equipped with two Fulmen calcium–lead batteries of 170 Ah, has a 24 V, 5.5 kW starter motor, and a 28 V, 90 A alternator. As a conventional vehicle, it runs with a 4-stroke diesel cycle, direct injection, with a variable geometry turbocharger and intercooler (6 cylinders). The actual image (a) and the vehicle representation on PyroSim (b) are shown in Figure 4 (qualitative approach).

In PyroSim, the vehicles were represented as parallelepipeds, where 5 faces show the constituent materials and 1 face (the top one) is labelled as the "burner", which is designated as the point of origin of the fire. This is a qualitative approach, as it does not accurately stand for the actual geometry of the vehicle. Moreover, in the model, the fire ignition point is found on the upper part of the vehicle, while in reality, the batteries are positioned on the underside. This is a limitation of the software, as it is not possible to

create wheels in the simulation, resulting in the vehicle being represented with a typical "box-like" shape resting on the ground. Representing the vehicle as "floating" with the "burner" surface placed underneath is also not valid. In this case, the heat generated by the thermal runaway would flow along the tunnel floor without the smoke rising upwards, leading to unreliable results, such as lower recorded temperatures in the tunnel or low pollutant concentrations, which compromise the validity of the experiment. The aspect of interest is the relative confrontation between the vehicles. The technical specifications of the two vehicles are shown in Table 2.

(**a**) (**b**)

Figure 4. (**a**) Image of the IVECO Stralis AS 260 vehicle; (**b**) its representation in PyroSim.

Table 2. Technical specifications of the vehicles used in the simulation.

Vehicle	Length [mm]	Width [mm]	Height [mm]	Engine Type	Battery Type	Installed Capacity [kWh]	Capacity [Ah]	Number of Batteries
SCANIA 25 P BEV	9965	2550	3109	Permanent magnet synchronous	Lithium ions	300	50	9
IVECO Stralis AS 260	9848	2550	3731	4-stroke with direct injection	Fulmen lead calcium		170	2

As can be seen in Table 2, the dimensions (length, width, and height) of the SCANIA and the IVECO vehicles are similar. In fact, the SCANIA is 0.117 m longer, has the same width (2.550 m), and is 0.622 m shorter in height compared to the IVECO, making the comparison particularly meaningful for assessing which of the two poses a greater environmental and health risk.

The PyroSim software required the input of the percentages and materials that make up the analysed vehicles. These were added to the simulation based on the document from the SCANIA company, specific to the construction of the ICEV and BEV trucks [20]. The percentages used and the materials adopted for the two vehicles are shown in Table 3.

The lithium-ion cells used in the SCANIA are NMC 622 (60% nickel, 20% manganese, 20% cobalt) because they are more common and efficient. The percentages of the minerals that make up these cells are shown in Table 4 [21].

Regarding the thermophysical properties of the materials used in the simulation, some of them have been simplified by considering only the components present in the highest percentage (such as glass in other materials, palladium in special metals, refrigerant in operating fluids, and copper in non-ferrous metals). The thermophysical properties of the materials that make up the adopted vehicles are listed in Table 5 [15,17,22].

Table 3. Composition of the vehicles used in the simulation.

Materials	SCANIA 25 P BEV Percentage	IVECO Stralis AS 260 Percentage
Steel	48%	57%
Cast iron	18%	22%
Aluminium	7.0%	5.0%
Cells	13%	
Non-ferrous metals (copper)	2.0%	1.9%
Operating fluids (coolant, engine oil, ...)	0.3%	1.0%
Polymers	9.6%	11.0%
Special metals (palladium)	0.1%	0.1%
Other materials (glass)	2.0%	2.0%

Table 4. Composition of NMC cells in the SCANIA BEV.

Mineral	Composition of the Cell	Percentage	SCANIA Percentage of Total
Graphite	Anode	28.10%	3.65%
Aluminium	Cathode, Casing, and Collectors	18.90%	2.46%
Nickel	Cathode	15.70%	2.04%
Copper	Collectors	10.80%	1.40%
Steel	Casing	10.80%	1.40%
Manganese	Cathode	5.40%	0.70%
Cobalt	Cathode	4.30%	0.56%
Lithium	Cathode	3.20%	0.42%
Iron	Cathode	2.70%	0.35%

Table 5. Thermophysical properties of the materials that make up the adopted vehicles.

Material	Density ρ [kg/m^3]	Thermal Conductivity k [W/mK]	Specific Heat c_p [kJ/kg·K]	Emissivity ε [-]
Steel	7500	22	0.502	0.79
Aluminium	2700	200	0.88	0.1
Cobalt	8900	100	0.42	0.93
Iron	7840	73	0.46	0.82
Cast Iron	7200	50	0.502	0.3
Graphite	2200	1600	0.72	0.9
Lithium	530	84.7	3.56	0.9
Manganese	7200	7.82	0.48	0.79
Nickel	8900	65	0.44	0.92
Palladium	12,020	71.8	0.244	0.15
Polymer	1000	15	1.67	0.9
Copper	8960	395	0.387	0.65
Coolant	1000	0.4	1.43	0.93
Glass	2200	1	0.677	0.85

The vehicles were placed in the middle of the two lanes and at the centre of the tunnel Figure 5 shows the top view of the SCANIA vehicle position in PyroSim (excluding the upper part of the tunnel).

Figure 5. Top view of the SCANIA vehicle position in the tunnel (yellow box).

2.4. HRRPUA and Ramp-Up Time

As mentioned in the previous paragraph, the upper part of the vehicles (parallel-footed in PyroSim) is a 'burning' surface, destined to be the source of the fire. The other faces are inert throughout the entire simulation time. The characteristic parameters of a burner are the HRRPUA and the rise time. The first (heat release rate per unit area) is the maximum thermal energy emitted during the fire per unit of the area considered [in kW/m^2], and it is calculated as follows:

$$HRRPUA = \frac{HRR_{max}}{A_{burner}} \quad (4)$$

As a function of the maximum HRR (heat release rate), the HRRPUA also depends on the type of fuel and the composition of the vehicle that is burning. In general, there is no universal formula that can calculate the maximum HRR for a vehicle of any type. Nevertheless, while in many cases, reference is made to examples in the literature or experimental data, for large EVs, equations are used to calculate the maximum power output in the event of a fire. This value is defined by the sum of the conventional NFPA value for a bus equipped with a diesel engine (around 20–30 MW) and the value [in kW] derived from the equation reported in [23]:

$$HRR_{max} = 2E_B^{0.6} \quad (5)$$

in which E_B is the battery capacity [in Wh].

The HRR_{max} value for the EV is 20.866 MW, obtained by summing 17 MW (a value close to the lower end of the NFPA range for diesel buses) and the result of Equation (5) with 300 kWh as the installed battery pack capacity. Lecocq et al. conducted a study on fires involving vehicles of similar size, where two different engines (conventional and electric) were installed in a tunnel [24]. They found the HRR_{max} values of 6.1 MW and 4.7 MW, respectively. By proportionally adjusting the HRR_{max} for the electric HGV based on these values, the input value used for the IVECO vehicle simulation is 27.081 MW. The adopted measures fall within the standards for large vehicles outlined in NFPA 502 (20–200 MW) and in the PIARC documents and French guidelines (20–30 MW) for tunnels and restricted-access areas [25,26]. Tables 6 and 7 show the experimental data derived from the NFPA 502 document and the standards from the older NFPA documents, PIARC, and the French guidelines.

Table 6. Experimental HRR_{max} data according to NFPA standard 502.

Vehicles	Peak HRR [MW]	Time to Peak HRR [min]
Passenger car	5–10	0–54
Multiple passenger car	10–20	10–55
Bus	25–34	7–14
Heavy goods truck	20–200	7–48

Table 7. HRR_{max} [in MW] of different vehicles according to the old NFPA, PIARC documents, and the French guidelines.

Vehicles	HRR_{max} PIARC [MW]	HRR_{max} French [MW]	HRR_{max} NFPA [MW]
1 small passenger car	2.5		
1 large passenger car	5		5
2–3 passenger cars	8	8	
Van	15	15	
Bus	20		20
HGV	20–30	30	20–30
Tanker	100	200	100

By dividing these quantities by the area of the burner surfaces, the HRRPUA [in kW/m^2] values were obtained and are reported in Table 8.

Table 8. HRRPUA and ramp-up time of the analysed vehicles.

Vehicle	HRR_{max} [kW]	Burner Area [m^2]	HRRPUA [kW/m^2]	t [s]
SCANIA-EV	20,866	25.41	821.16	429
IVECO-ICEV	27,082	25.11	1078.43	162

The other parameter affecting the burner is the rise time (or ramp-up time), i.e., the time it takes for the thermal energy released to reach the maximum value (HRR_{max}) in case of a fire. Wang et al. conducted studies on lithium-ion batteries with a capacity of 50 Ah (like those used in the SCANIA vehicle) and found a rise time of 429 s [27]. Cheong et al. [28] performed an analysis of fires caused by conventional vehicles inside tunnels and found that the ramp-up time of an HGV during ignition is 162 s. The ramp-up times used [in s] are reported in Table 8.

2.5. Mesh

In the context of fire modelling in tunnels, the grid encompasses both the tunnel and the involved vehicle, enabling the simulation to be conducted and the results to be analysed. A key parameter influencing the accuracy and efficiency of the simulation is the subdivision of the grid. Decomposing the computational domain into multiple sub-grids allows for increased spatial resolution, as the total number of cells is higher than that of a single grid, while simultaneously reducing computational time, since each sub-grid can be assigned to a separate processor, using parallel computing. In particular, the sub-grid enclosing the vehicle affected by the fire is typically discretised with a higher number of cells compared to other regions, as it is where more intense thermal phenomena and the release of toxic substances occur, necessitating greater resolution and longer computational times. Considering the most severe fire scenario, in which the ignition source is located at the centre of the tunnel, and assuming that significant variations in physical quantities, such as temperature, are confined to a few metres from the ignition point, a central sub-grid of 120 m in length with a finer resolution has been adopted. The lateral sections, where the phenomena are less significant and of lower interest for analysis, have been discretised using sub-grids of 400 m in length, characterised by a lower number of cells (coarse grid), ensuring a balance between accuracy and computational efficiency.

The division of the tunnel into the adopted meshes is shown in Figure 6.

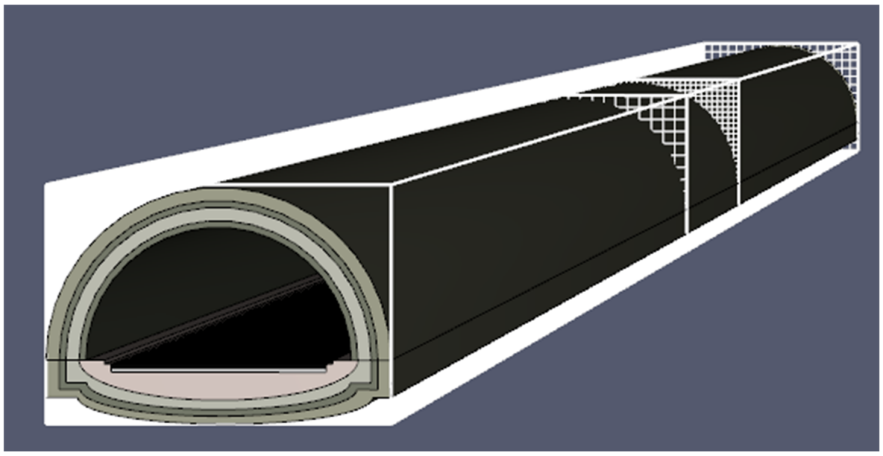

Figure 6. Meshes (highlighted in white) of the analysed case study.

A useful quantity for determining the appropriate number of cells, ensuring both good accuracy and a reasonable computational time for the model, is the characteristic fire diameter (D*) [11]. This parameter [in m] is calculated using Equation (6):

$$D^* = \left(\frac{\dot{Q}}{\rho_\infty c_p T_\infty \sqrt{g}} \right)^{\frac{2}{5}} \quad (6)$$

where $\dot{Q}$ indicates the HRR_{max} of the battery [in kW], ρ_∞ represents the air density (1.204 kg/m^3), T_∞ indicates the ambient temperature (293.15 K), c_p represents the specific heat capacity of the ambient air (1.005 kJ/kg·K), and g represents the acceleration due to gravity (9.81 m/s^2). The characteristic fire diameter is used in the simulation to determine the number of cells that make up a mesh. The larger the value of this parameter, the "finer" the mesh will be. To achieve a good balance between accuracy and computational cost, the cell size Δx should be between $\frac{D^*}{5}$ and $\frac{D^*}{20}$ [29].

The characteristic fire diameters for the three vehicles are provided in Table 9.

Table 9. Characteristic fire diameters of the analysed vehicles.

Vehicle	Q [kW]	D* [m]	Mesh D*/5 [m]	Mesh D*/10 [m]	Mesh D*/20 [m]
SCANIA	20,866	3.23	0.65	0.32	0.16
IVECO	27,082	3.59	0.72	0.36	0.18

To compare the results of the simulations for the three vehicles and to provide moderate accuracy to the model, a unique cell length Δy was chosen for both cases, set at 0.70 m for the meshes less affected by the phenomena resulting from the fire and 0.35 m for the central mesh (which requires more detail). The cell lengths along the y-direction (Δy) and z-direction (Δz) are derived from the ratios with Δx, resulting in cell dimensions of 0.7005 × 0.6842 × 0.6923 m (for Δx of 0.70 m) and 0.3509 × 0.3421 × 0.3462 m (for Δx of 0.35 m). The number of cells and the lengths of the meshes are provided in Table 10.

Table 10. Number of cells and mesh length of the analysed case study.

Mesh	Tunnel Length Section [m]	Cell Size Δx [m]	Total Number of Cells
Mesh 1	0–400	0.7	141,037
Mesh 2	400–520	0.35	337,896
Mesh 3	520–920	0.7	141,037

According to the FDS user manual [30], the software uses a Poisson solver based on a fast Fourier transform (FFT). This implies that optimal grid divisions are constrained to the form $2^u\ 3^v\ 5^w$, where u, v, and w are integers. In this case, the number of cells assigned to the central mesh (337,896) follows the rule since it is divisible by powers of 2 and 3. By contrast, the number associated with the side meshes (141,037) is prime and could cause undesirable results. However, Caliendo et al. [31] demonstrated that cell lengths, assigned to meshes characterizing a long tunnel and ranging from 0.4 m to 0.2 m (such as a Δx of 0.35 m for the lateral meshes), result in simulation errors of less than 1%.

The surfaces of the meshes that do not interact with each other were considered "open" in the mesh boundary vent, meaning they are characterised by the external atmospheric conditions outside the solid layers that make up the tunnel.

2.6. Combustion Reaction

The combustion reaction of the batteries is the key element for generating the fire starting from the burner surfaces of the vehicles in PyroSim. By adopting a simple chemical reaction in the FDS, it is necessary to identify a single compound as the fuel. For BEVs, the substances involved in the combustion reaction are numerous and depend on the type of battery used. Shen et al. [32] identified the fuel components that make up the various battery types in the event of a thermal runaway NMC and LFP event in an inert atmosphere. Specifically, the substances characterizing an NMC 622 battery are CO_2 (35.3%), CO (32.4%), H_2 (23.4%), CH_4 (4.1%), C_3H_8 (3.1%), and C_3H_6 (1.7%). Figure 7 shows the pie chart containing the percentages of the fuels that make up the NMC 622 cell.

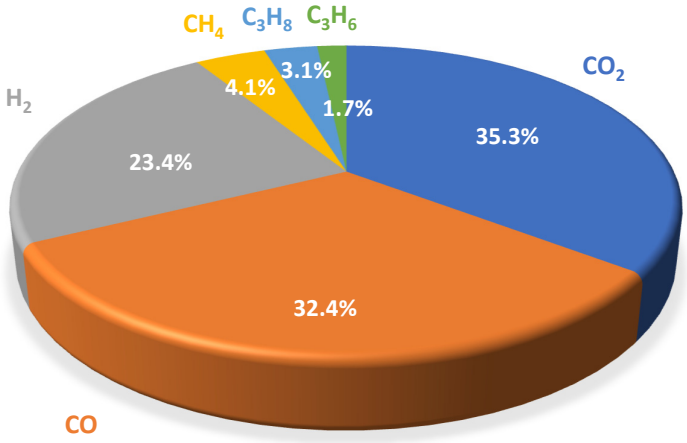

Figure 7. Composition of the NMC 622 cell used in the simulation.

Regarding the conventional vehicle, Betiha et al. [33] discovered that diesel fuel is composed of 75% aliphatic hydrocarbons (paraffins and cycloalkanes) and a small number of aromatic hydrocarbons (olefins and alkylbenzenes). Although the chains that compose diesel range from $C_{10}H_{20}$ to $C_{15}H_{28}$, the substance $C_{12}H_{23}$ can be considered as the average fuel in the simulation [34]. Unlike other substances present in the PyroSim database, the thermal data and chemical composition for diesel fuel were manually entered. The data and are provided in Table 11.

Table 11. Characteristics of the diesel fuel used in the simulation.

Type of Fuel	Chemical Composition	Specific Heat at 20 °C	Density	Vaporisation Temperature	Melting Temperature	Vaporisation Heat	Formation Enthalpy
Diesel fuel	$C_{12}H_{23}$	1900 kJ/kg·K	850 kg/m^3	210 °C	−8.1 °C	326 kJ/kg	6700 kJ/mol

Another variable to include in the simulation is the heat of combustion, defined as the amount of heat released during combustion processes. For the conventional vehicle, this quantity is equal to the lower heating value (LHV) of diesel fuel (42,600 kJ/kg) [35]. For EV batteries, however, there is no single value because it depends on various parameters, including the type and size of the cells. Sturm et al. [36] conducted a series of tests on BEV fires in tunnels with an installed capacity of around 80 kWh and found an energy release of 2893 MJ. Considering that the cells of a BMW full electric car weigh about 15% of the vehicle's mass, and using a Toyota bZ4x pure (with an empty weight of 1920 kg) as a reference [37,38], the heat of combustion H [in kJ/kg] was calculated using Equation (7):

$$H = \frac{Q}{m} \quad (7)$$

where Q is the amount of energy released [in kJ] and m is the mass of the battery [in kg]. The value for the SCANIA vehicle was calculated by proportionally adjusting the result of Equation (4), which is 10,045.14 kJ/kg, with the battery capacities (80 kWh and 300 kWh), resulting in the value adopted in the simulation (37,669.27 kJ/kg). The final parameters to include for the combustion reaction of the two vehicles are the mass fractions of carbon monoxide (CO) and the soot produced during combustion. The assigned values primarily affect the amount of smoke emitted from the vehicle's burner surface. Based on tests conducted on conventional vehicles and EVs in fires within confined spaces [39], the values are 0.025 kg_{CO}/kg_{fuel} and 0.035 kg_{soot}/kg_{fuel} for an ICEV, and 0.032 kg_{CO}/kg_{fuel} and 0.044 kg_{soot}/kg_{fuel} for a BEV.

2.7. Ambient Boundary Conditions and Simulation Time

The chosen simulation duration is 600 s, as it represents the maximum safe evacuation time for personnel in the event of a fire in a tunnel, based on the research by Wang et al. [40]. The parameters that describe the external environment entered into PyroSim and characterise the faces of the meshes that do not interact with each other are a temperature of 20 °C, a pressure of 101,325 Pa, an oxygen concentration in the air of 23% by mass, a CO_2 concentration in the air of 0.0595% by mass, a relative humidity of 40%, a wind speed of 0 m/s, and a gravitational acceleration of 9.81 m/s^2.

2.8. Devices

One of the parameters analysed is the temperature reached on the ceiling in case of a vehicle fire. To carry out this analysis, 93 solid-phase devices were inserted into the simulation, positioned along the top of the tunnel at 10 m from each other. Figure 8 shows the positions of the ceiling temperature detection probes in the analysed case study.

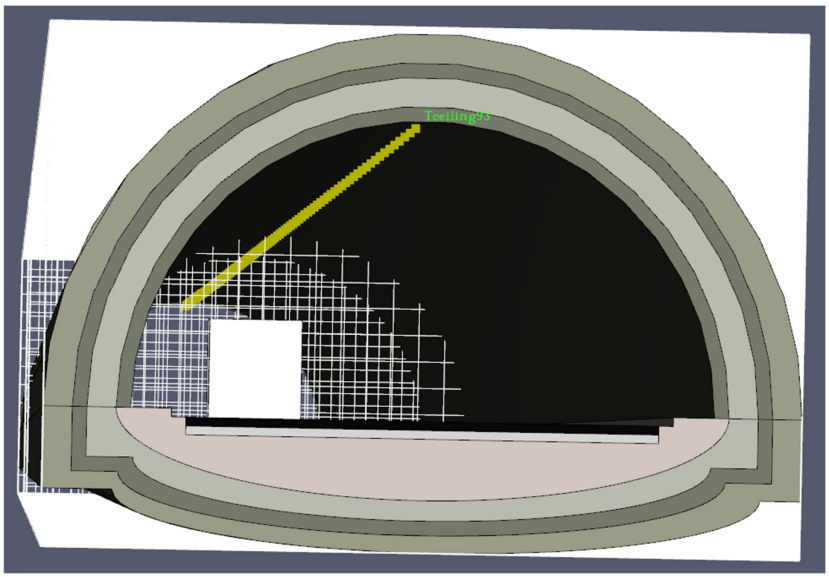

Figure 8. Temperature devices $T_{ceiling}$ (in yellow) along the tunnel.

For a better understanding of the temperature distribution in space, 2D slices were used along the three directions of the computational space. Specifically, along the x and y directions, they were placed on the vehicle's median planes, while along the z direction, a detection height of 4 m was chosen. For further analysis, 61 check points were positioned along the y-axis at the centre point of the vehicle, passing through its surface and spaced 0.10 m apart. Figure 9 illustrates the position of the devices in the calculation space.

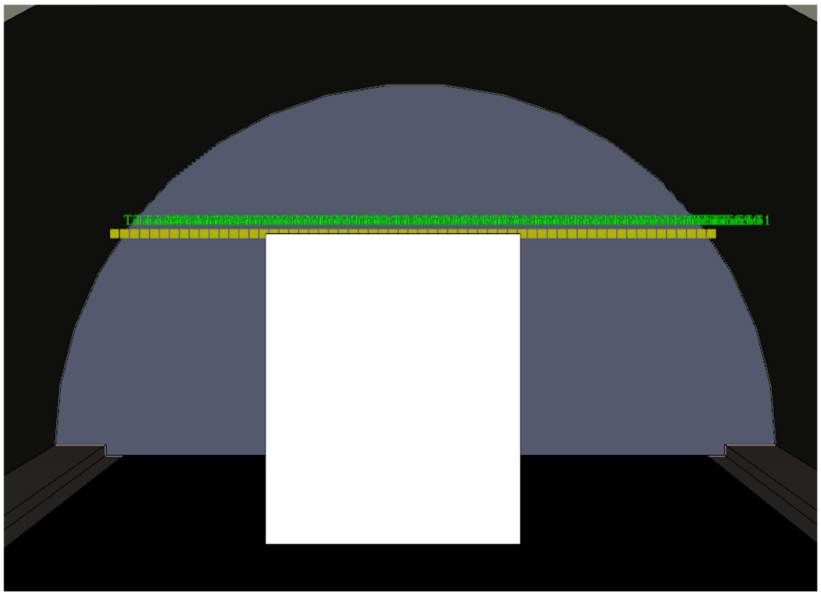

Figure 9. T_{airy} devices (in yellow) in the considered space.

To evaluate the smoke concentration (reduction of visibility) in the tunnel, 47 smoke detectors (gas-phase devices) were placed along the first half, spaced 10 m apart. To assess the health risks to people fleeing, these detectors were placed in the simulation at a height of 1.70 m from the ground (the average height of an adult). Figure 10 shows the position of the devices along the first half of the tunnel.

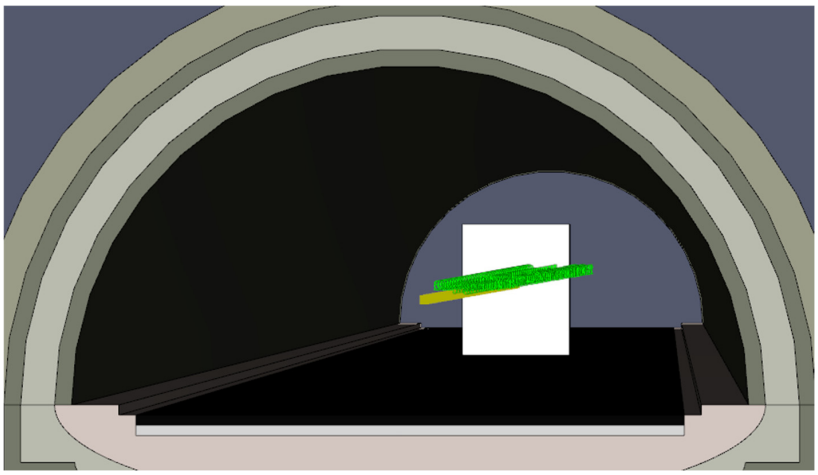

Figure 10. Smoke detectors (in yellow) in the tunnel.

In the case where fans are present in the tunnel, a 2D slice was used along the median y-axis of the vehicle to measure the airflow velocity along the tunnel.

2.9. Longitudinal Mechanical Ventilation

To size the fans, two parameters were calculated. The first is the critical velocity at which air is introduced into the tunnel. According to NFPA 2020 [25], this is defined as the minimum constant velocity required to prevent backlayering (a phenomenon in which smoke moves in the opposite direction of the incoming air) from the fire site. In the design of a ventilation system, the parameter values used in the calculation formulas, such as HRRmax or temperature, are those associated with the vehicle fire scenario that yields the highest values, ensuring the system is sized for the most demanding conditions. To set up the formula for calculating the critical velocity, it used the following relation:

$$\frac{\dot{Q}}{\rho_a c_p T_a g^{\frac{1}{2}} H'^{\frac{5}{2}}} > 0.15 \left(\frac{H'}{W}\right)^{-\frac{1}{4}} \quad (8)$$

where H' represents the tunnel height (5.15 m), W represents the tunnel width (10 m), $\dot{Q}$ represents the HRR_{max} of the vehicle [in kW], ρ_a represents the density of the ambient air (1.2 kg/m^3), T_a represents the ambient air temperature (293.15 K), and g represents the acceleration due to gravity (9.81 m/s^2). Once the inequality is satisfied, the velocity u [in m/s] is found by considering both the grade factor as a function of the actual tunnel slope (−0.78%) and the following formula:

$$u = 0.43 e^{\left(-\frac{L_b}{18.5H}\right)} \sqrt{gH} \quad (9)$$

where L_b is the backlayering length (which is 0 m in the case of critical velocity). The second parameter calculated is the total pressure losses p_{tot} [in Pa] that the system must compensate for, and it is obtained from the following equation [41]:

$$p_{tot} = p_i + p_f + p_{dir} + p_{ar} + p_{or} + p_o + p_b + p_m \quad (10)$$

where p_i represents the pressure loss [in Pa] at the tunnel entrance, p_f represents the pressure loss [in Pa] due to friction on the tunnel walls, p_{dir} represents the pressure loss [in Pa] along the flow direction in the pipes in the ventilation system, p_{ar} represents the area pressure loss [in Pa] due to the distribution of flow through the various fans, p_{or} represents the pressure loss [in Pa] due to openings or cracks through which air can flow into the ventilation system, p_o represents the pressure loss [Pa] at the tunnel exit, p_b represents the pressure loss [Pa] due to the buoyant forces of the air, and p_m represents the pressure loss [Pa] due to atmospheric conditions (wind and barometric pressure differences). The values of the losses to be compensated by the ventilation system are calculated based on several parameters, including the critical airspeed, the geometric characteristics of the ducts, the location of the fire and the tunnel, the number of vehicles present, the maximum HRR of the vehicle causing the greatest damage, the atmospheric conditions at the entrance and exit, and the physical properties of the environment in question. These latter characteristics depend on the average air temperature measured on the surface of the vehicle. Subsequently, the flow rate to be fed into the tunnel $\dot{V}$ [in m^3/s] is obtained from the following formula:

$$\dot{V} = A_t c \quad (11)$$

where A_t is the tunnel cross-sectional area (40.56 m^2) and c is the incoming air velocity. The total power of the ventilation system [in kW] can be calculated as follows:

$$P = \dot{V} \frac{p_{tot}}{1000} \quad (12)$$

Based on the calculated values, the designed tunnel ventilation system can compensate for all losses and achieve at least the minimum power.

3. Results

3.1. SCANIA

The HRR resulting from the simulation conducted on the large BEV is characterised by two of the three main phases (propagation and stationary fire) that describe the trend of energy released following a fire [42]. Figure 11 shows an initially increasing trend for the first 400 s, with a peak of almost 20,000 kW, followed by a constant phase for the remaining

time. This trend mainly depends on the HRRPUA, with ramp-up time used as an input (821.16 kW/m^2 and 429 s, respectively), which represent the coordinates of the HRR$_{max}$, and the chosen combustion heat (37,669.27 kJ/kg), which determines the length of the second phase and the compactness of the curve. A value (expressed in kJ/kg) larger than the HRR$_{max}$ (20,866 kW) increases the onset time of the decay phase, leading to the display of the other two phases within 600 s of simulation and affecting many physical properties. Of these, the most significant is the increase in internal air temperature in the confined space. Similar orders of magnitude between the HRRmax and the heat of combustion result in a relatively constant amount of thermal energy released over time during each phase. This results in a more compact curve.

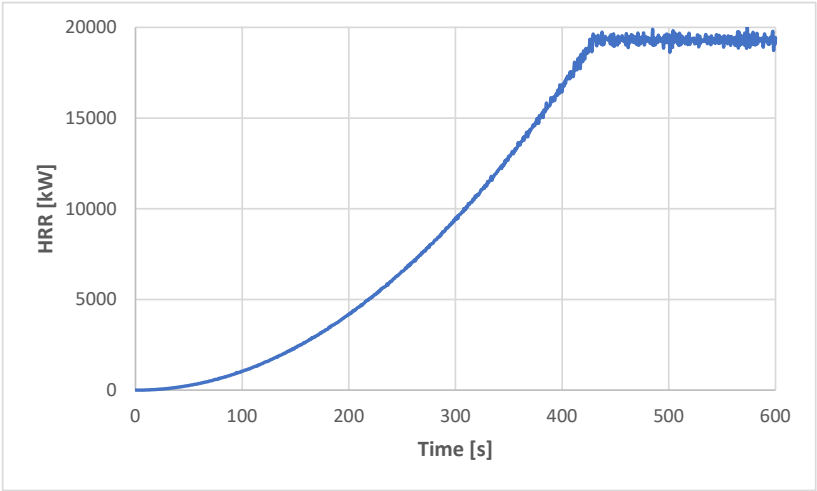

Figure 11. HRR of the SCANIA vehicle.

Figure 12 shows a symmetrical trend of the ceiling temperature along the tunnel at each analysed time point, caused by the geometric characteristics of the vehicle and the tunnel being the same along the median axis. The peaks found at 460 m are due to the presence of the vehicle, the source of the fire, at that point. The time points evaluated are 60 s (the most critical time to ensure safety in the event of an explosion or particularly intense fire), 180 s (the time when the fans are switched on [41]), 430 s (the time when the HRR$_{max}$ is reached), and 600 s (the end of the simulation). Figures 13–15 show the temperature distributions recorded on the 2D slices at the end of the simulation.

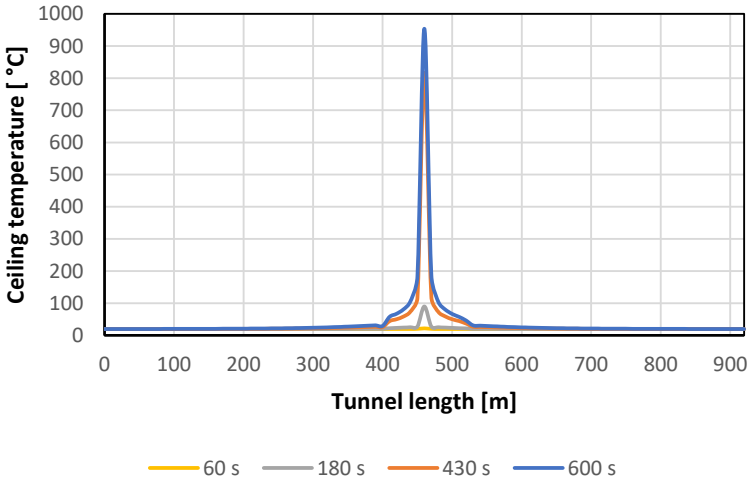

Figure 12. Ceiling temperature of the SCANIA tunnel simulation at different time points.

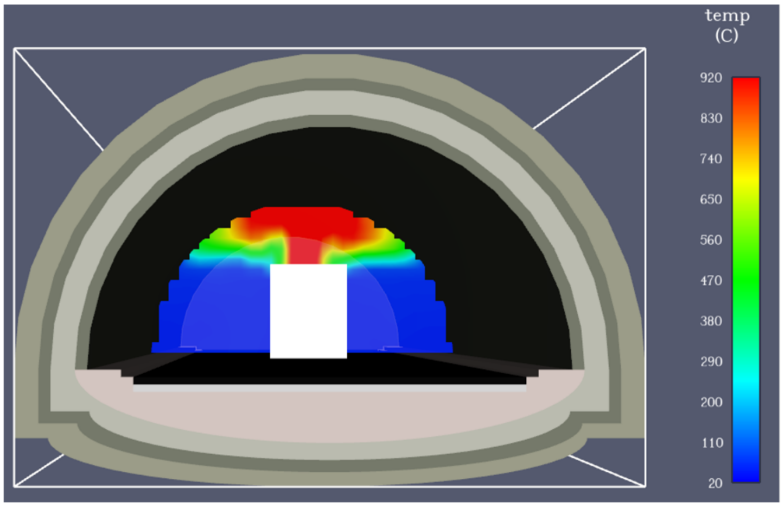

Figure 13. Two-dimensional temperature of the SCANIA vehicle at X = 460 m and 600 s of simulation.

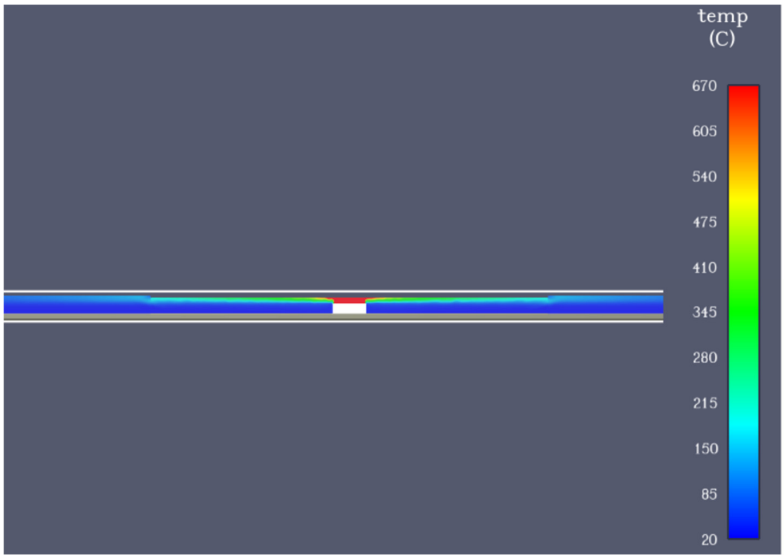

Figure 14. Two-dimensional temperature of the SCANIA vehicle at Y = 6.158 m and 600 s of simulation.

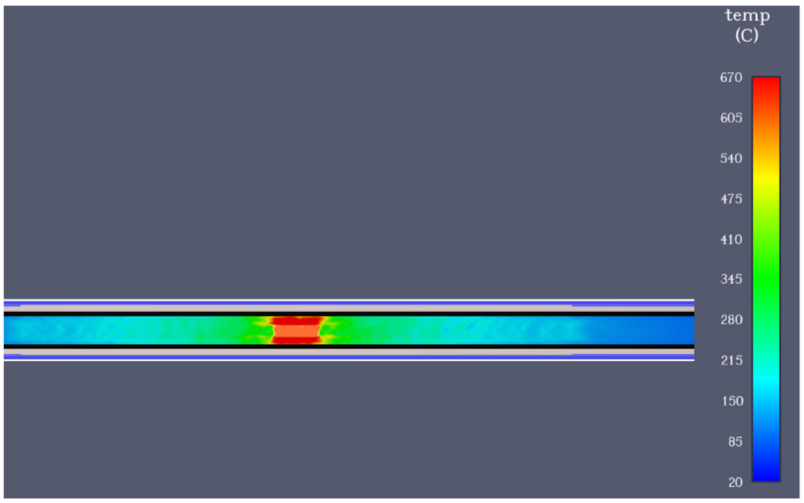

Figure 15. Two-dimensional temperature of the SCANIA vehicle at Z = 4 m and 600 s of simulation.

In Figure 14, the maximum peaks of 953.58 °C and 816.93 °C are shown in the moments after reaching the HRR_{max}, and 89.93 °C is noted three minutes after the fire ignition. However, one minute after the event, no significant temperature change from room temperature (20 °C) is observed.

Figure 13 shows the temperature rise above the SCANIA vehicle and illustrates the pinnacle with maximum temperatures of 920 °C and temperatures up to 110 °C at a height of ~1.7 m. Figure 14 shows a longitudinal section of the tunnel and a well-developed temperature stratification in the vicinity of the burning truck. Figure 15 illustrates the temperatures at a height of 4 m. To demonstrate the temperature trends, Figure 16 shows the 2D probe trends at X = 460 m at 60, 180, 430 and 600 s from the start of the simulation. After 60 s of simulation (a), no significant temperature changes are observed. 180 s after ignition (b), the plume becomes visible, with temperatures fluctuating between 200 °C and 290 °C. Once the HRR_{max} is reached, after 430 s (c), the entire volume of the tunnel above the SCANIA truck is filled with smoke, as indicated by the significant rise in temperatures in this area. Once this state is reached, it remains until the end of the simulation (600 s) (d).

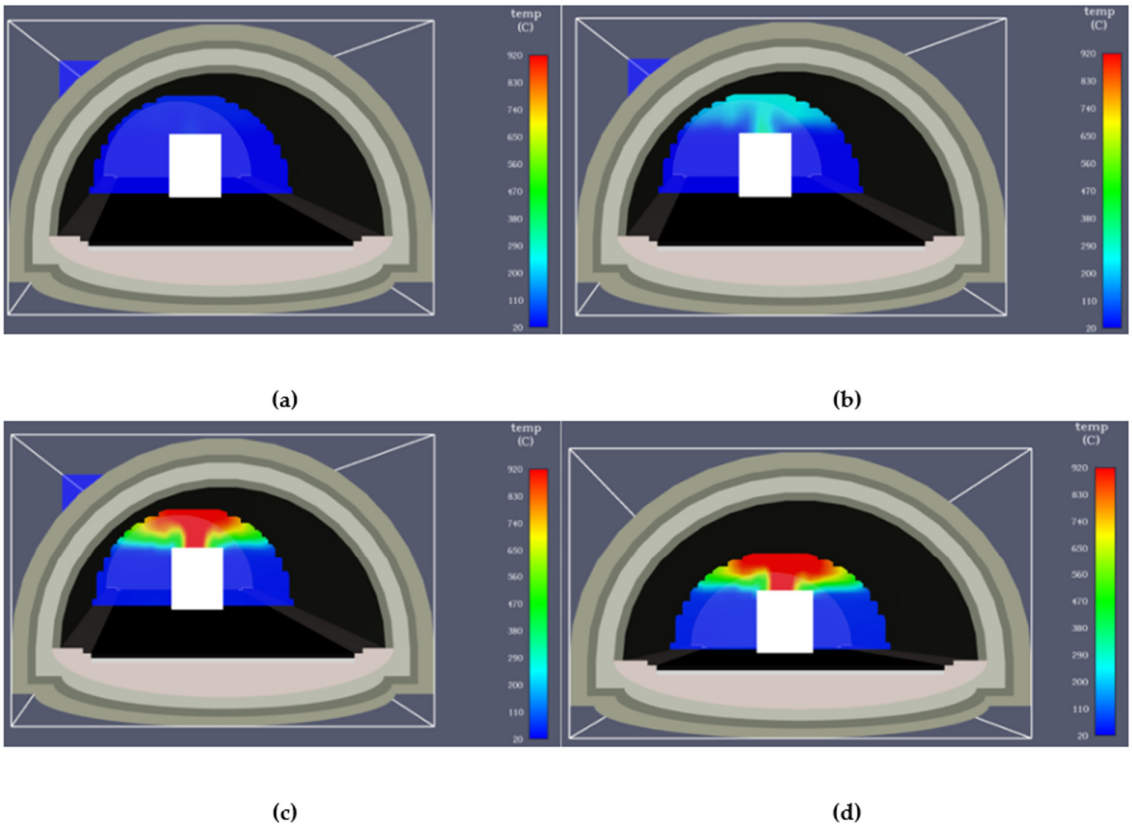

Figure 16. Two-dimensional temperature of the SCANIA vehicle: (**a**) at X = 460 m and 60 s of simulation; (**b**) at X = 460 m and 180 s of simulation; (**c**) at X = 460 m and 430 s of simulation; (**d**) at X = 460 m and 600 s of simulation.

Verifying that the trend is symmetrical from left to right of the vehicle, Figure 17 shows the temperature distribution at different time points, recorded by 29 probes, as a function of distance from the centre (near the vehicle surface). A decreasing trend is observed at the different time points, followed by a constant phase in the remaining part of the graph. Between 60 and 180 s, the temperature decreases to around 20 °C from 1.30 m (half the width of the vehicle). After 430 and 600 s, the reduction terminates at 1.90 m with values of 91.7 °C and 95.3 °C, respectively. The maximum temperature recorded on the surface of the SCANIA vehicle at the end of the simulation (1185.7 °C) is very similar to that measured

after 430 s (1171.6 °C). By contrast, there is a significant increase during the propagation phase, evidenced by the temperature increase between 60 and 180 s (from 70.98 °C to 363.1 °C). These temperature values are in agreement with the experimental work of Held et al. [9] and of Kang et al. [43]. The thermal runaway of EVs was studied, and the results showed similarities and orders of magnitude to support the results.

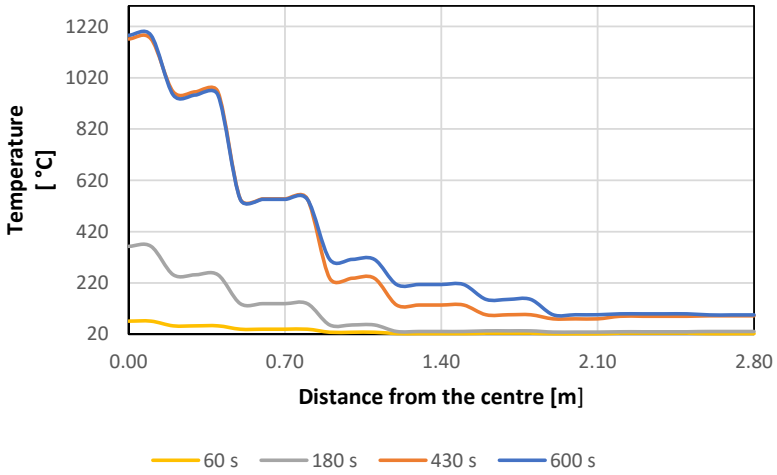

Figure 17. Air temperature near the vehicle surface (SCANIA vehicle) as a function of the distance from the centre.

One of the most important quantities to analyse in the event of a vehicle fire is visibility. Figure 18 shows the simulation results at different considered time points. After 60 s (a), it is possible to see a concentration of smoke exclusively in the upper part of the tunnel. After 180 s (b), there is an increase in smoke that covers half of the vehicle, significantly reducing the visibility of the surrounding environment and causing health issues for people fleeing. After 430 s (c) and 600 s (d), the smoke concentrations in the tunnel are nearly identical, covering the interior of the structure.

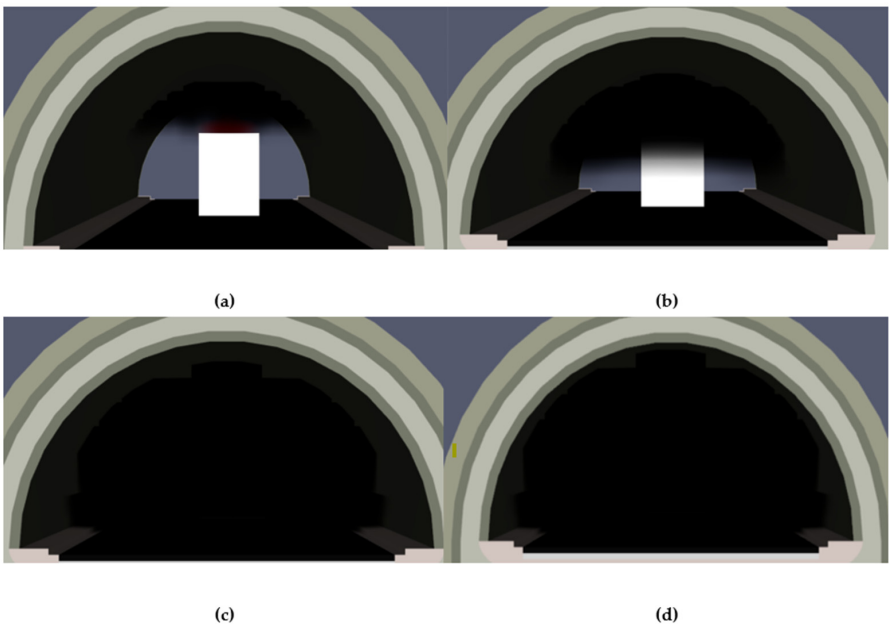

Figure 18. Tunnel visibility: (**a**) after 60 s; (**b**) after 180 s; (**c**) after 430 s; (**d**) after 600 s.

Figure 19 shows the graphs of smoke concentrations [in %m] as a reduction of visibility, as a function of the distance from the centre of the vehicle, recorded by the detectors at different time points. A negligible amount of smoke is seen after 60 s and 180 s, with a

peak of 1.71% at 50 m from the SCANIA vehicle. However, once HRR_{max} is reached, the percentage increases within the first 280 m from the centre of the vehicle, with a peak of 39.86% at 180 m. A similar trend is observed at the end of the simulation, with an increase in smoke concentration over 380 m of the tunnel, where the maximum, recorded at 200 m, reaches 86.52%. The minimum observed at 60 m is due to the presence of the probe at the boundary between two meshes with different resolutions, causing measurement instability effects (see the FDS manual). According to the FDS user guide [30], these turbulence effects are related to the presence of obstacles (such as the layers constituting the tunnel) that form at the interfaces of two meshes with different resolutions. The probes at boundary points will record temperature or smoke concentration values that will result in irregularities in the trends of these quantities along the tunnel (reduction of visibility). The peaks observed in the later time points are a result of the smoke diffusion along the tunnel ceiling and the early descent of the vapours further away from the vehicle.

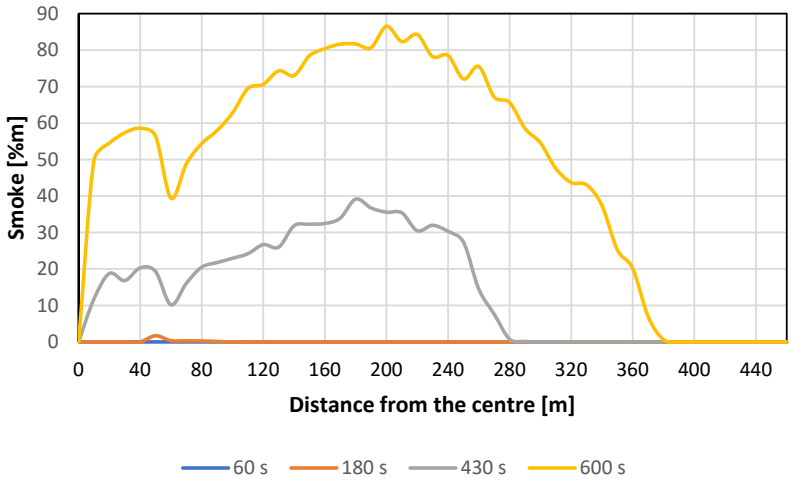

Figure 19. Smoke concentration (reduction of visibility) in the tunnel due to the SCANIA vehicle as a function of the distance from the centre.

3.2. Comparison Between the SCANIA and the IVECO

Two large vehicles of similar size and weight (SCANIA and IVECO) were compared to determine the fire-related consequences for an electric vehicle and a conventional vehicle. Figure 20 shows a comparison of the HRR curves of both simulations. The main differences concern the ramp-up time and the HRR_{max}.

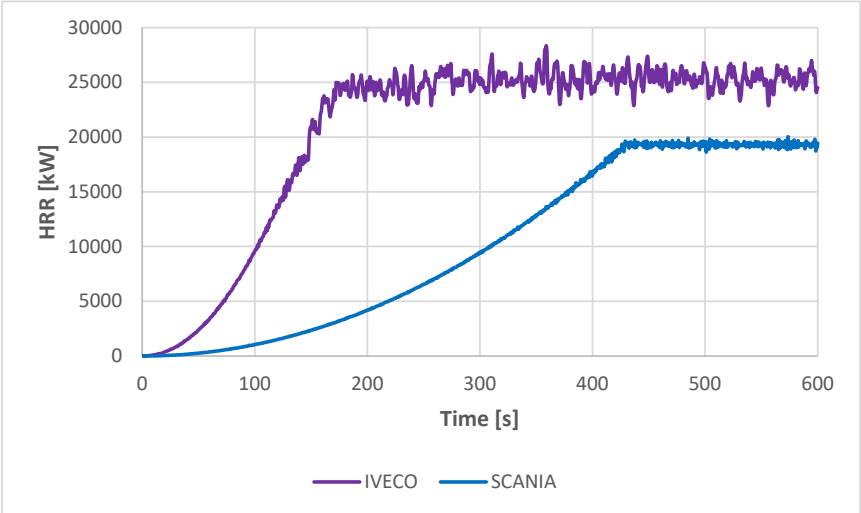

Figure 20. HRR of the SCANIA vehicle (in blue) and the IVECO vehicle (in purple).

Figure 21 shows the temperatures measured on the ceiling as a function of tunnel length for both the IVECO and the SCANIA simulations. The time instances considered are 162 s (the moment when the IVECO vehicle reaches the HRR_{max}) and 600 s (the end of the simulation). As seen for the SCANIA simulation, the maximum temperatures recorded in the IVECO simulation reached 460 m from the beginning of the tunnel (the centre of the vehicle and the point of ignition of the fire). The distribution is symmetrical with respect to the midpoint of the graph, given the same tunnel and vehicle geometric conditions. Unlike the EV, which shows a significant increase in temperature at the ceiling at the peak (rising from 70.5 °C after 162 s to 953.58 °C after 600 s), the in-fire of the IVECO vehicle results in a more limited temperature increase at the centre of the vehicle (rising from 616.6 °C after 162 s to 617.1 °C after 600 s). This implies that the diesel vehicle reaches the maximum temperature value at the end of the propagation phase, where the thermal properties change significantly over time. Furthermore, in the IVECO simulation, a longer section (up to 120 m) is shown with higher ambient temperatures than in the analysis performed on the SCANIA vehicle (up to 100 m).

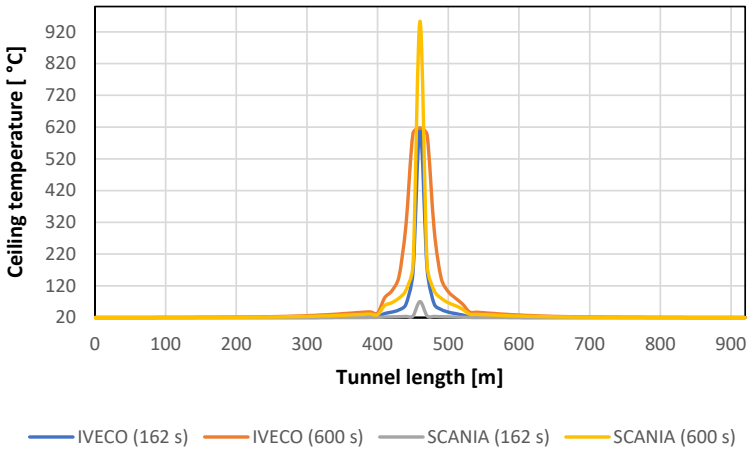

Figure 21. Ceiling temperature of the tunnel with the SCANIA and the IVECO vehicles at different time instances.

Figures 22–24 show the images recorded by the 2D slices regarding the temperature measured at different planes of the calculation space.

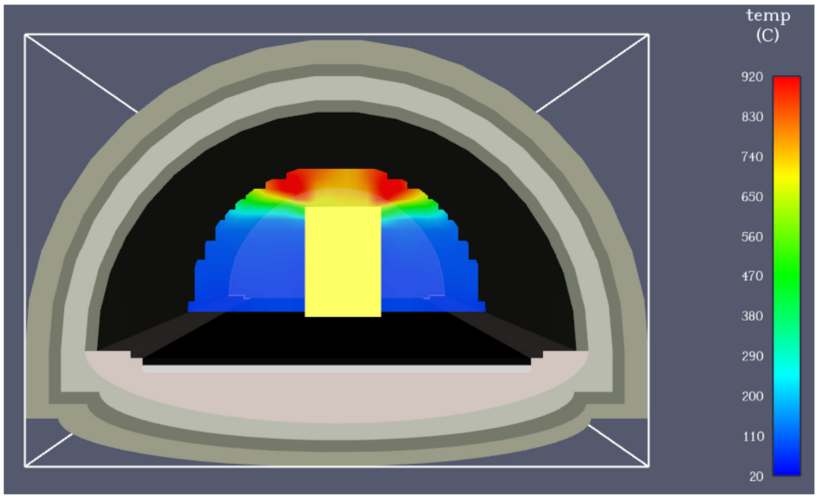

Figure 22. Two-dimensional temperature of the IVECO vehicle at X = 460 m and 600 s of simulation.

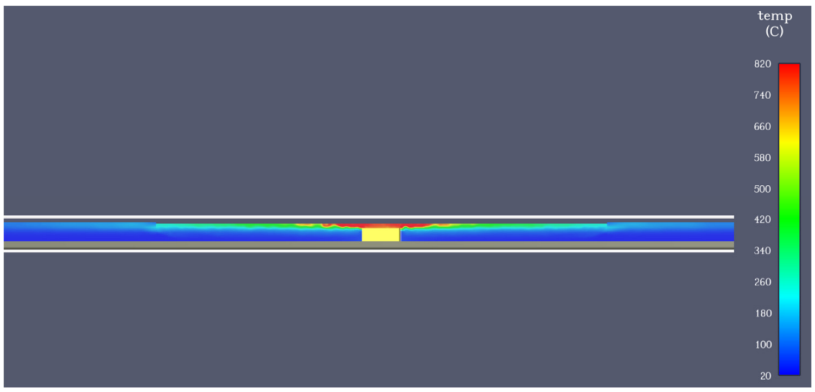

Figure 23. Two-dimensional temperature of the IVECO vehicle at Y = 6.158 m and 600 s of simulation.

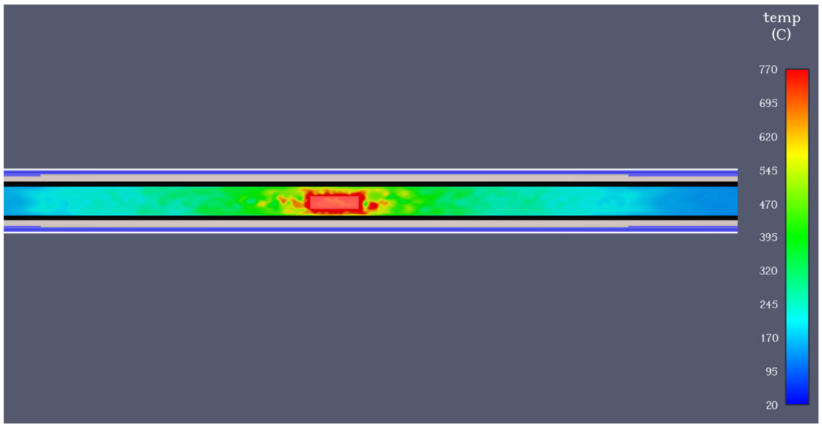

Figure 24. Two-dimensional temperature of the IVECO vehicle at Z = 4 m and 600 s of simulation.

Figure 22 shows a ceiling temperature peak of 920 °C, followed by a decreasing temperature trend towards the lower layers. Still high temperatures (110 °C) are observed near the vehicle. Figure 23 shows an increase in temperature in both the central and side meshes, with a minimum of 180 °C. Figure 24 shows a limited increase in temperature at a height of 4 m in the part of the tunnel closest to the vehicle (up to 60 m away), with a peak of 770 °C in the centre. Unlike the SCANIA vehicle, where the maximum temperature recorded by the probes along the y- and z-axes is the same, the analysis on the IVECO vehicle showed a difference of 40 °C between the two. This transition from 820 °C at the ceiling to 770 °C at 4 m above the ground implies less heat with increasing height above the ground, due to a low HRR value at that time (as shown by the curve in Figure 20). For more details on the temperature trend over time, Figure 25 shows the results of the simulation conducted on the probe installed at X = 460 m after 162 s and after 600 s.

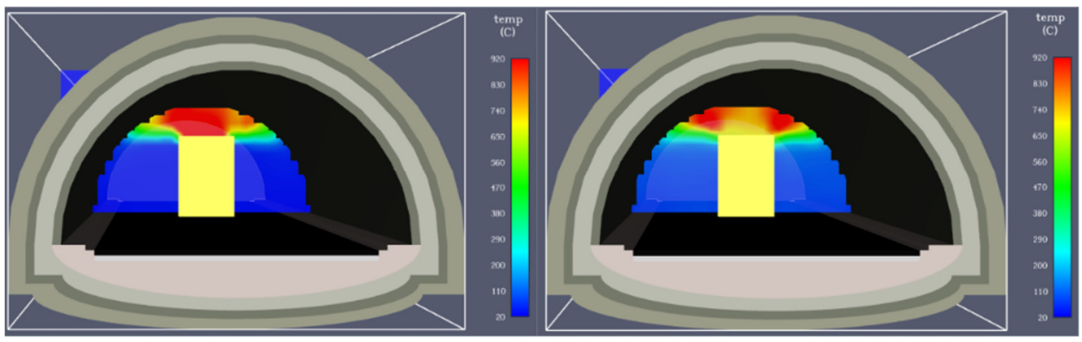

(**a**) (**b**)

Figure 25. Two-dimensional temperature of the IVECO vehicle: (**a**) at X = 460 m after 162 s; (**b**) at X = 460 m after 600 s.

Figure 25a,b show a localised decrease in temperature in the central part of the tunnel (above the vehicle) during the steady-state fire phase. Above the vehicle, a temperature between 830 °C and 920 °C is recorded at time t = 162 s, while at the end of the simulation, a temperature between 650 °C and 740 °C is observed. As one can see in Figures 23 and 24, this change is due to a low HRR value at that moment. Figure 26 shows the temperatures measured by the 29 probes placed along the x-axis, which intersect the surface of the IVECO and the SCANIA vehicles as a function of the distance from the latter at different time instances. In the SCANIA vehicle, throughout approximately 430 s, a temperature increase at zero distance is observed, nearly quadrupling (from 308.4 °C to 1185.7 °C). By contrast, the simulation conducted on the IVECO vehicle showed a decrease in the centre of the fire (from 1128.25 °C to 676.77 °C). This trend is attributed to the thermal energy released, which, at a time equal to 600 s, depends on a lower HRR value (24,506.1 kW) compared to the maximum found at 162 s (27,081.88 kW). The trends observed in the IVECO simulation are different from those obtained in the previous cases. Along the vehicle's burner surface (up to 1.10 m), after 162 s, the temperature decrease is not uniform concerning the distance from the centre, showing several peaks at certain points. Farther from the surface (beyond 1.10 m), a constant section at 277.78 °C is evident, followed by an increasing section with a maximum of 610.89 °C, and a decreasing section down to 425.28 °C. At the end of the simulation, however, the trend is nearly constant around 660 °C, with brief intervals where peaks of 955 °C and lows of 543.75 °C are reached. As seen in Figure 25, a constant temperature trend along the upper part of the vehicle (up to 1.10 m) is noticeable, due to a uniform decrease in the HRR. Unlike the SCANIA vehicle, diesel fuel generates a broader heat distribution in the case of a fire, extending up to 1.60 m. At moments when the thermal energy reduces (such as at 600 s), the temperature in the section between 1.20 m and 1.50 m does not decrease compared to the measurements recorded along the surface of the vehicle. The heat that had previously reached the top of the tunnel (when the HRR was higher) descended along the vault, causing an increase in temperature in the section between 1.20 m and 2.80 m. At the end of the simulation, the temperature in this latter interval shows a non-uniform trend, depending on the HRR and the heat present in the air.

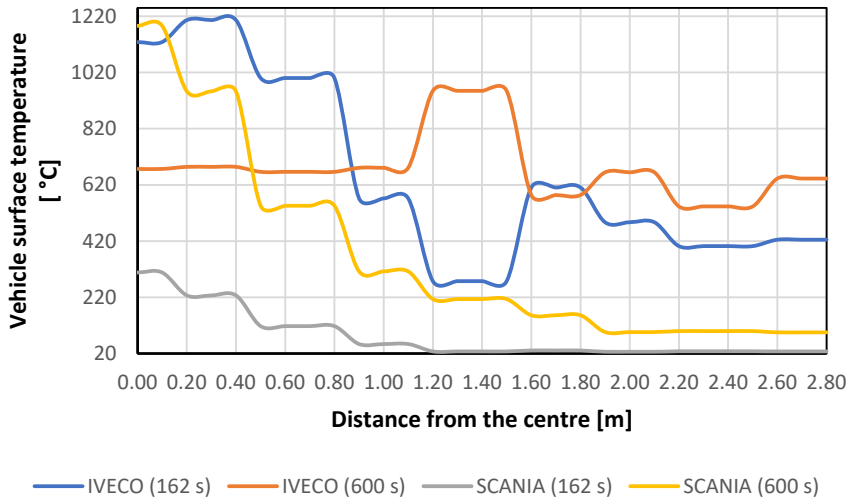

Figure 26. Air temperature near the vehicle surface, the SCANIA vehicle and the IVECO vehicle as a function of the distance from the centre.

To understand the temperature behaviour along the line passing through the vehicle's surface, Figure 27 shows the temperature trends over time recorded by the probes closest to and farthest from the vehicle.

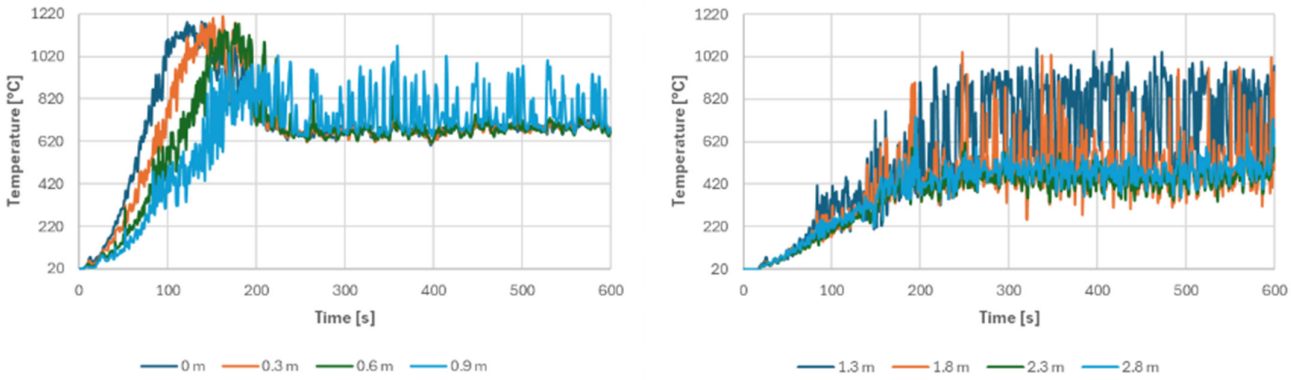

(**a**) (**b**)

Figure 27. (**a**) Temperature of the IVECO vehicle near the surface and (**b**) far from the surface as a function of time.

In the probes near the surface (a), a generally increasing trend followed by a decreasing phase that ends at a constant average value in the last minutes of the simulation can be observed. The maximum temperature reached (1206.26 °C) was recorded at 0.3 m from the centre of the vehicle. Although average trends are evident in all the probes, the heat generated by the diesel combustion reaction varies over time, causing temperature oscillations in the graph. As seen in Figure 26, at 162 s, the temperature in the first 1.10 m from the centre of the vehicle decreases after releasing the maximum possible thermal energy, while at 600 s, a nearly constant value is reached for all probes. In the probes farther from the surface (b), a generally increasing trend is observed, with greater oscillations compared to those recorded by the probes closer to the vehicle. The maximum temperature reached (1052.54 °C) was measured at 1.3 m from the centre of the IVECO vehicle. As seen in Figure 26, at 162 s and 600 s, the temperature, starting from 1.30 m from the centre, varies according to the HRR at that specific moment in time. Figure 28 shows the visibility in the IVECO vehicle simulation at the different time instances considered. It is possible to observe an increase in the amount of smoke inside the tunnel. Although the lower part of the tunnel and the vehicle can be seen after 162 s (a), by the end of the simulation (b), the visibility is zero. As in the case of the SCANIA vehicle, the increased smoke in the air poses health risks to people that escape.

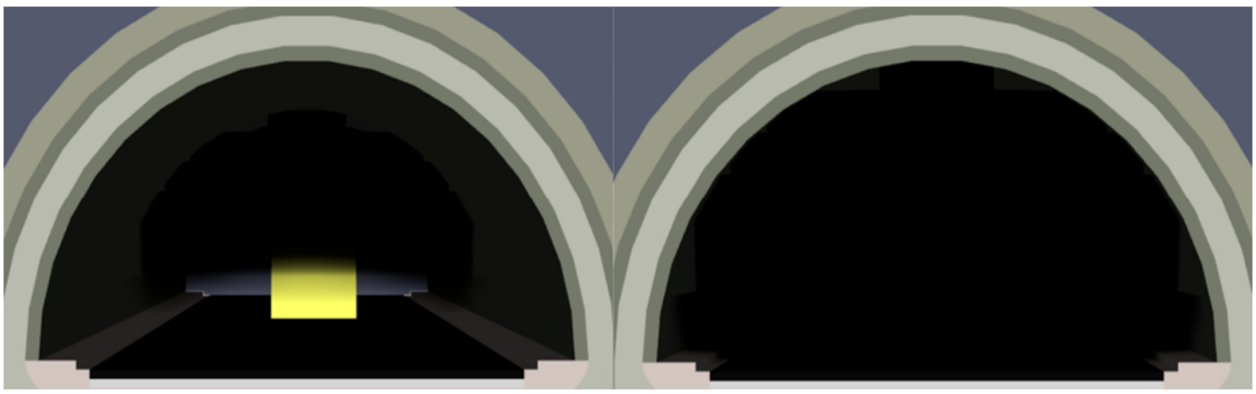

(**a**) (**b**)

Figure 28. (**a**) Smoke produced by the IVECO vehicle after 162 s and (**b**) after 600 s from the fire origin.

Figure 29 shows the smoke concentrations (reduction of visibility) measured in the SCANIA and the IVECO simulations as a function of the distance from the centre. At the end of the simulation, the maximum measured smoke concentration reduction of visibility (93.89%) is higher than the SCANIA simulation (86.52%). The same observation holds

at 162 s after the fire begins, where a maximum of 2.32% of pollutants is observed in the IVECO simulation, compared to 0.37% found in the EV simulation. In addition to the type of fuel used, the observed percentages also depend on the mass fractions adopted as input parameters for soot and CO (0.025 kg_{CO}/kg_{fuel} and 0.035 kg_{soot}/kg_{fuel} for an ICEV, and 0.032 kg_{CO}/kg_{fuel} and 0.044 kg_{soot}/kg_{fuel} for a BEV). Furthermore, after 600 s, the pollutant gases from the diesel vehicle nearly occupy the entire tunnel (440 m compared to the 380 m covered by smoke from the SCANIA). This results in decreased visibility and an increased health risk. Unlike the simulation conducted on the SCANIA vehicle, no significant instabilities were recorded in the IVECO vehicle analysis at the boundary between the lateral meshes and the central mesh (60 m from the centre), preventing the relative minima on the graph.

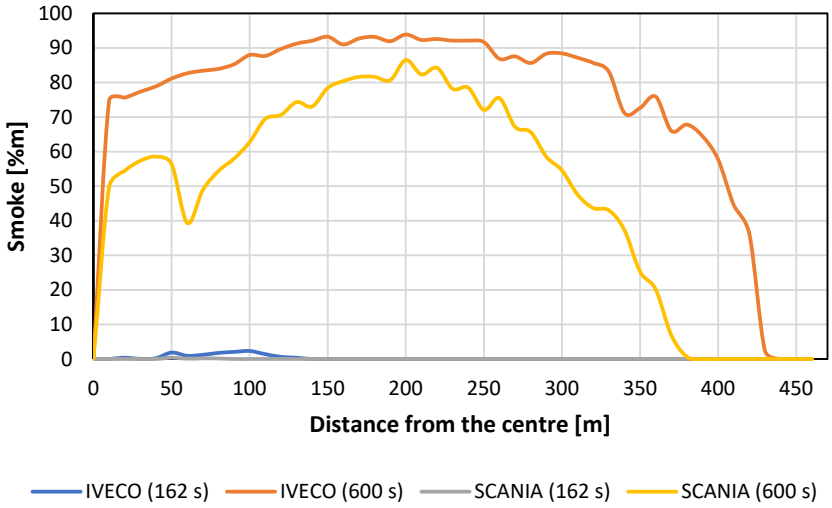

Figure 29. Smoke concentration (reduction of visibility) in the tunnel due to the SCANIA and the IVECO vehicles as a function of the distance from the centre.

3.3. SCANIA with Fans

From the maximum temperatures measured by the 2D probes (920 °C along x, 820 °C along y, and 770 °C along z), those recorded along the surface of the vehicle (1271.89 °C), and the high concentration of smoke produced (with a maximum concentration of 94.53%), the IVECO vehicle was found to cause the highest impact related to human health and the tunnel structure. The physical properties of the tunnel, useful for fan sizing, were considered with an average air temperature on the surface of the conventional vehicle equal to 700 °C (measured by the 1D and 2D probes). From Equations (8)–(12), the critical air velocity was found to be 3.16 m/s, the total system loss was found to be 2670.81 Pa, and the minimum power to be met was found to be 346.65 kW. To compensate for all losses and to achieve the minimum power obtained, 12 AIRONN 710 jet fans were simulated, grouped in pairs on the tunnel ceiling, spaced 129.78 m apart. These fans are 1.92 m long, 0.91 m wide [44]. They are characterised by a flow rate of 14.9 m^3/s, a single power of 30 kW, and produce a net thrust of 670 N with an air velocity of 37.6 m/s. In addition to the geometric characteristics and the airflow rate for sizing the fans in PyroSim, the last parameters to be entered into the simulation are the activation time and the ramp-up time. Considering that the temperature recorded at 162 s is high, it was assumed that the system would start operating at a lower time. For this reason, a value of 60 s was chosen (the time at which the maximum temperature on the surface of the IVECO vehicle reaches 700 °C). The time interval between fan activation and reaching full fan speed is 20 s. Figure 30 shows the real image (a) and the PyroSim representation (b) of the jet fan.

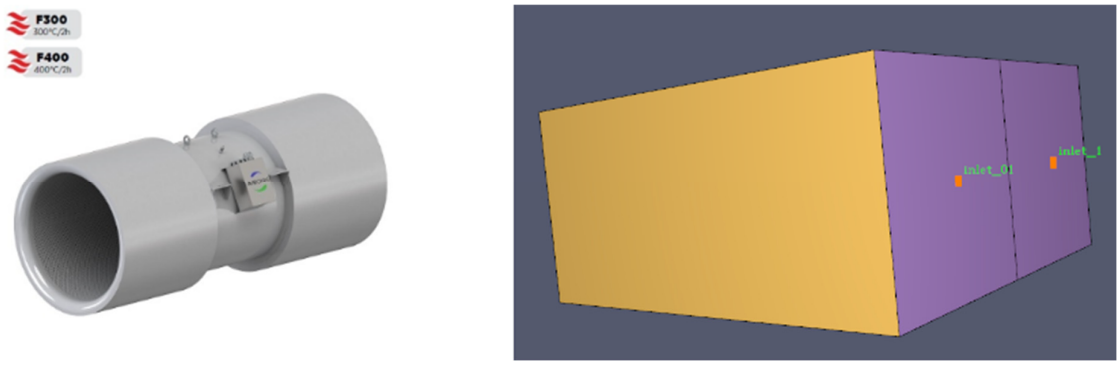

(**a**) (**b**)

Figure 30. (**a**) Image of an AIRONN 710 jet fan and (**b**) a reproduction of a pair of fans in PyroSim.

To assess the benefits that the ventilation system has on the tunnel in the event of a vehicle fire, several parameters were measured and compared with the results obtained in the case without fans. The time instances analysed are 150 s (50 s after the fans' ramp-up time is reached) and 600 s (end time of the simulation). Figure 31 shows the temperatures measured on the ceiling as a function of the tunnel length, in the case where the fans are present, and in the case where they are absent.

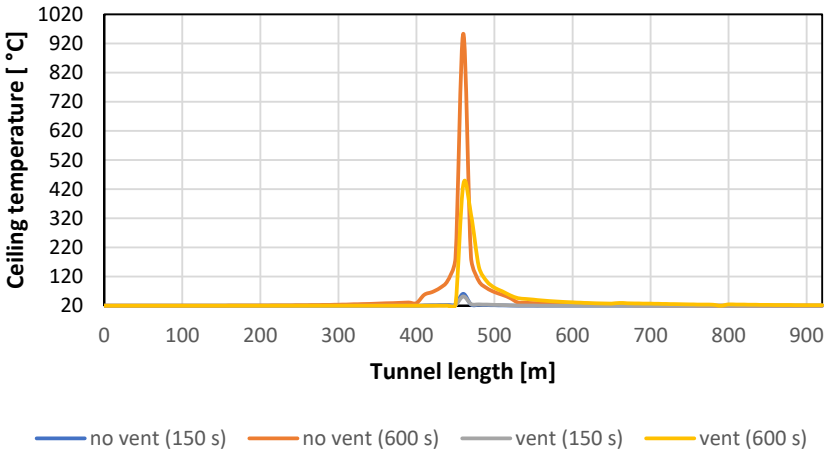

Figure 31. Ceiling temperature of the SCANIA tunnel simulation (with and without fans) at different time instances.

In Figure 31, no temperature variation can be observed at 150 s along the tunnel from the beginning of the simulation. After 50 s from the activation of the fans at full power, a slight temperature difference is observed at the centre (decreasing from 60.87 °C to 52.06 °C), due to the intake of cold air along the top of the vehicle. After 600 s, the effect of ventilation in the SCANIA simulation reduces the maximum temperature by about half (from 953.58 °C to 435.78 °C). The cold air introduced by the fans helps redistribute the thermal energy released in the section between 460 and 900 m (the tunnel exit section), creating the asymmetric distribution highlighted in the graph. This allows the first 460 m of the tunnel (the entrance section) to maintain a temperature of 20 °C. Figures 32–34 show the temperatures recorded by the 2D probes in the different planes of the computational domain.

Figures 32–34 highlight significant reductions in the maximum temperatures at the end of the simulation. In the first figure, the temperature reaches a maximum of 520 °C (compared to the 920 °C recorded in Figure 13) in a smaller area than in the case without fans. In Figure 33, the heat displacement caused by the fans results in an asymmetric distribution along the tunnel, with a maximum temperature of 520 °C (compared to 670 °C recorded in Figure 14). In Figure 34, the position of the fans on the tunnel ceiling helps shift the

heat upward, reaching higher temperatures (maximum of 570 °C), but still lower than those measured in the base case (with a peak of 670 °C visible in Figure 15). Figures 35 and 36 show the smoke distributions along the computational domain after 150 s and 600 s, respectively.

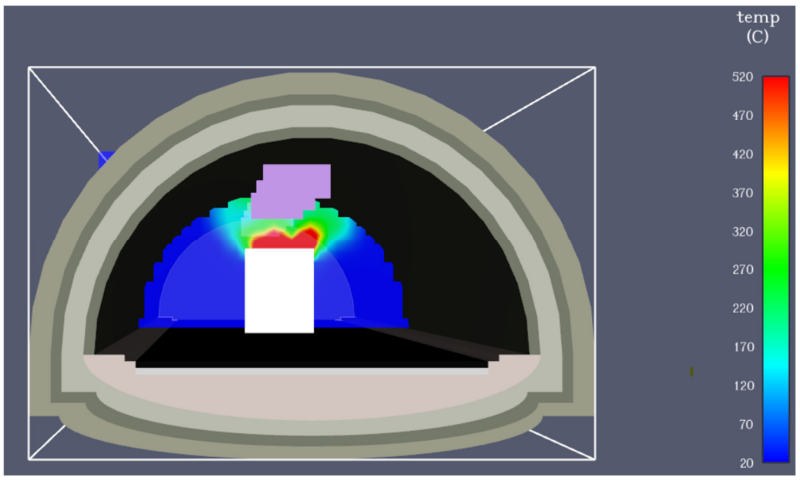

Figure 32. SCANIA vehicle temperature (with fans) 2D at X = 460 m and 600 s of simulation.

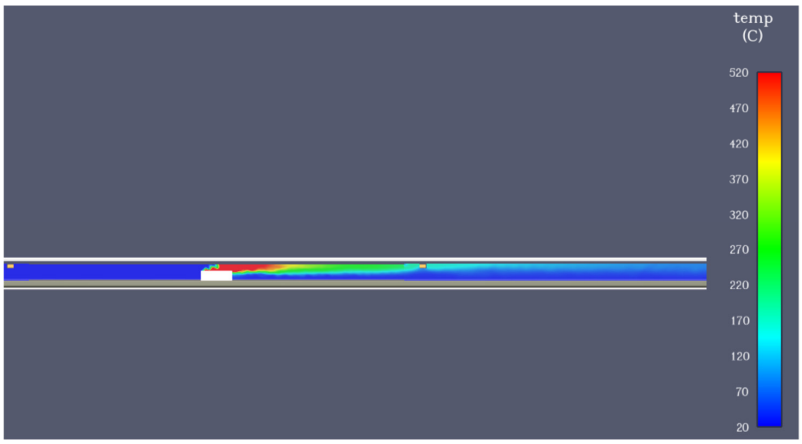

Figure 33. SCANIA vehicle 2D temperature (with fans) at Y = 6.158 m and 600 s of simulation.

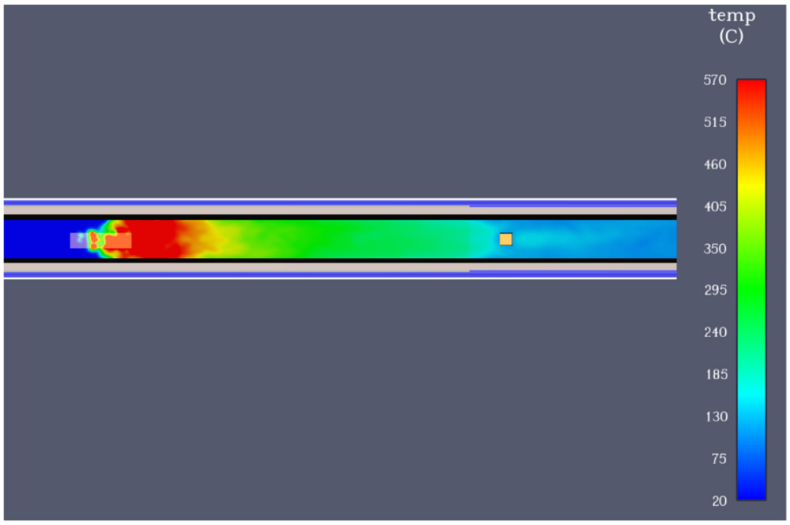

Figure 34. SCANIA vehicle 2D temperature (with fans) at Z = 4 m and 600 s of simulation.

Figure 35. Smoke produced by the SCANIA vehicle (with fans) after 150 s of simulation.

Figure 36. Smoke produced by the SCANIA vehicle (with fans) after 600 s of simulation.

In Figures 35 and 36, an increase in smoke concentration (reduction of visibility) along the tunnel is observed, due to the gradual increase in the combustion reaction rate over time. After 50 s from the achievement of the ramp-up time, the elimination of the backlayering phenomenon in the central fan is not noticeable. However, at the end of the simulation, no black smoke is observed in the first 460 m (the tunnel entrance section), demonstrating the correct sizing of the adopted fans and ensuring a comfortable environment with clean air. Figure 37 shows the airflow velocity trends along the tunnel recorded by the 2D probe after 150 s and 600 s.

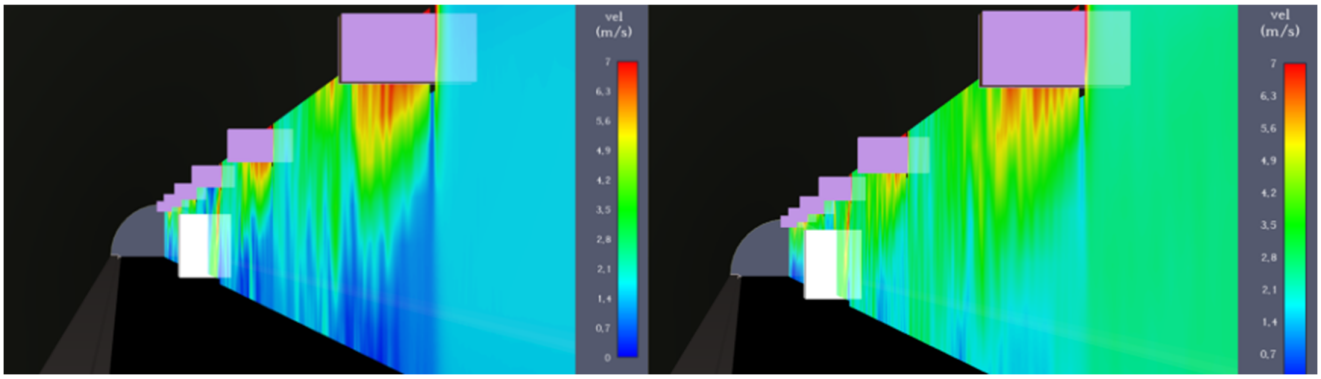

(**a**) (**b**)

Figure 37. SCANIA vehicle 2D velocity (with fans): (**a**) at Y = 6.158 m and 150 s of simulation; (**b**) at Y = 6.158 m and 600 s of simulation.

Starting from the first 100 s (a) of the simulation (ramp-up time), the airflow velocity near the fans reaches 7 m/s due to the input flow rate (14.9 m^3/s). After 150 s, a decreasing velocity trend is observed along the lower part of the tunnel (down to 0.7 m/s). This is due to the height of the fans from the ground, which primarily displace air from the upper layers, thereby affecting the lower layers, which are rich in smoke. The velocity observed on the right side of the image (1.6 m/s) corresponds to the velocity recorded in the initial sections at the tunnel entrance. At the end of simulation (b), the same trend as the previous figure is evident, with an increase in velocity in the lower part (up to 1.6 m/s), determined by the increase in smoke. The velocity recorded at the entrance is also higher (2.5 m/s), due to a greater displacement of air around the adjacent fans.

4. Discussion

EVs have been designed to replace conventional vehicles to reduce pollutant emissions in a particularly energy-intensive sector. Among these, large vehicles represent a greater environmental hazard due to the high thermal energy released in the event of a fire. To assess the risk, a CFD simulation was used to model the consequences of a thermal runaway in a confined space, such as a highway tunnel. The analysis carried out on the 920 m long Rimazzano Tunnel, with a simulation time of 600 s, revealed an increase in temperature on the vehicle's surface, reaching 1185.76 °C, and on the ceiling, peaking at 953.58 °C. Moreover, the smoke produced reached its maximum at 200 m from the vehicle (86.52%), spreading up to 380 m from the centre of the vehicle. Analysing the behaviour of a vehicle with a diesel engine, with similar dimensions and weight to the EV, showed a maximum

temperature on the surface 6.77% lower and on the ceiling 33.70% lower compared to the conventional vehicle (1271.9 °C and 631.9 °C, respectively). The maximum temperatures measured on the surfaces of both vehicles do not fully comply with the standards defined by studies on the fire risk of HGV ICEVs and BEVs. These studies report maximum temperatures for a conventional car (800–1000 °C) [45–47] and for an EV (900–1100 °C) [43,48]. This difference is due to the materials involved and the combustion heat values and the HRR_{max} used, which result in different temperatures (such as the maximum found at the centre of the IVECO ICEV at 1271.9 °C and that found at the centre of the SCANIA BEV at 1171.60 °C). By contrast, the maximum temperatures recorded on the ceiling fall within the temperature ranges defined by the EUREKA 499—FIRETUN tests conducted on vehicle fires in long tunnels [49]. According to this source, the maximum values reached on the ceiling range from 200 °C to 1100 °C for the HRR_{max} values between 6 and 128 MW. The maximum values found in the IVECO vehicle (631.90 °C with the HRR_{max} of 27,081.9 kW) and the SCANIA vehicle (953.58 °C with the HRR_{max} of 20,866 kW) are therefore consistent with the results highlighted by the research. The maximum smoke production of the electric truck is 8.47% lower than the diesel truck (94.53%). The analyses also revealed a smoke spread of up to 440 m from the conventional vehicle, reducing visibility and harming the health of people escaping. Furthermore, implementing improvement strategies, such as ventilation systems, offers additional benefits, such as directing the smoke towards the tunnel exit, thereby minimizing respiratory damage to escaping people and reducing the high temperatures recorded on the tunnel ceiling (by 54.32%), preventing structural materials from melting, and allowing rescue operations to be carried out with a high level of safety. The ventilation system complies with EU Directive 2004/54/EN, which applies to all tunnels on the trans-European road network longer than 500 m (such as the Rimazzano Tunnel), requiring the implementation of safety measures in the event of an incident to ensure a minimum level of safety for road users [10]. Indeed, although a different value (3.2 m/s) was used for the fan sizing, the input flow rate allowed a speed (7 m/s) that surpassed the critical limit (3.16 m/s) and avoided smoke backlayering at the tunnel entrance. This speed value falls within the range defined by the PIARC document (6–8 m/s) [50], which identifies the range adopted for longitudinal ventilation, limiting the damage that toxic substances can cause by interacting with the external environment. In this study, at zero wind speed, the maximum smoke concentration was 80% (reduction of visibility).

5. Conclusions

This study provides qualitative insights into the fire dynamics of large electric and conventional vehicles. The results indicate that electric vehicles produce comparable thermal output to fossil fuel vehicles, though differences in smoke dispersion and visibility were observed. The BEVs and ICEVs produce an HRR curve, which shows peak values of 20.87 MW for the SCANIA BEV and 27.08 MW for the IVECO ICEV. While the ICEV fire reaches a slightly higher peak HRR, both vehicle types fall within the same order of magnitude. At 600 s, the maximum smoke concentration (visibility reduction) reached 93.89% for the ICEV and 86.52% for the BEV, with smoke from the ICEV spreading over 440 m of the tunnel compared to 380 m for the BEV. These results show some confrontation, and the need for experimental tests to validate these results is emphasised. Current knowledge on toxic emissions and fire behaviour in large BEV incidents remains limited, underscoring the need for further research, particularly experimental validation. The effectiveness of the ventilation system is demonstrated by the significant reduction in ceiling temperature and visibility.

Given the distinct fire safety implications across vehicle types, it is essential to adapt and design fire scenarios accordingly. The findings also highlight the importance of implementing advanced safety systems—such as ventilation, smoke control, and suppression

technologies—within tunnel infrastructure. Future work should focus on real-scale fire scenarios and assess the performance of additional safety measures to support risk mitigation in complex environments.

Author Contributions: Conceptualization, R.D., D.P., and D.F.; methodology, R.D. and D.P.; software, R.D.; formal analysis, R.D.; data curation, R.D.; writing—original draft preparation, R.D.; visualization, R.D.; supervision, D.P. and D.F. All authors have read and agreed to the published version of the manuscript.

Funding: This research received no external funding.

Data Availability Statement: Data will be provided on request.

Conflicts of Interest: The authors declare no conflicts of interest.

Nomenclature

Symbol	Unit	Description
HGV		Heavy Good Vehicle
BEV		Battery Electric Vehicle
ICEV		Internal Combustion Engine Vehicle
FDS		Fire Dynamics Simulator
HRR	kW	Heat Release Rate
PM	ppmv	Particulate Matter in ppm by volume
SO_2	ppmv	Sulphur Dioxide
NO_x	ppmv	Nitrogen Oxides
EV		Electric Vehicle
GHG		Greenhouse Gas
EU		European Union
WTW		Well-To-Wheel
IEA		International Energy Agency
CFD		Computational Fluid Dynamics
CAD		Computer Aided Drafting
BIM		Building Information Modelling
IFC		Industry Foundation Classes
PHEV		Plug-in Hybrid Electric Vehicle
VLES		Very Large Eddy Simulation
NMC		Lithium Nickel–Manganese–Cobalt Oxides
HRRPUA	kW/m^2	Heat Release Rate Per Unit Area
NFPA		National Fire Protection Association
PIARC		World Road Association—Association Internationale Permanente des Congrès de la route (AIPCR)
CO_2	kg/kg_{fuel}	Carbon Dioxide
CO	kg/kg_{fuel}	Carbon Monoxide
H_2	kg/kg_{fuel}	Hydrogen
C_3H_8	kg/kg_{fuel}	Propane
CH_4	kg/kg_{fuel}	Methane
C_3H_6	kg/kg_{fuel}	Propylene
ρ	g/cm^3	Density
t	s	Time
u	m/s	Velocity
$\dot{m}_b'''$	$kg/s/m^3$	Net Heat Flux
p	Pa	Pressure
g	m/s^2	Acceleration
f_b	N	External Force

τ_{ij}	N/m^2	Stress Tensor
h	J/kg	Enthalpy
$\dot{q}'''$	W/m^3	Heat Per Unit Volume
$\dot{q}'''_b$	W/m^3	Energy for evaporation
$\dot{q}''$	W/m^2	Heat Flux
ε	W/m^3	Dissipative function
A_{burner}	m^2	Burner area
E_B	Wh	Battery capacity
D^*	m	Characteristic Fire Diameter
$\dot{Q}$	kW	HRR_{max} of the battery
ρ_∞	kg/m^3	Air density
c_p	kJ/kg·K	Specific heat
T_∞	K	Ambient temperature
H	kJ/kg	Heat of combustion
m	kg	Mass of the battery
Q	kJ	Energy released
H'	m	Tunnel height
W	m	Tunnel width
ρ_a	kg/m^3	Density of the ambient
L_b	m	Backlayering length
p_{tot}	Pa	Total loss
p_i	Pa	Inlet loss
p_f	Pa	Wall friction loss
p_{dir}	Pa	Flow direction loss
p_{ar}	Pa	Flow area loss
p_{or}	Pa	Orifice's loss
p_o	Pa	Outlet loss
p_b	Pa	Buoyancy loss
p_m	Pa	Meteorological loss
$\dot{V}$	m^3/s	Flow rate
A_t	m^2	Cross-section area
c	m/s	Air velocity
P	kW	Power of the ventilation system

References

1. Alanazi, F. Electric Vehicles: Benefits, Challenges, and Potential Solutions for Widespread Adaptation. *Appl. Sci.* **2023**, *13*, 6016. [CrossRef]
2. Helmers, E.; Marx, P. Electric cars: Technical characteristics and environmental impacts. *Environ. Sci. Eur.* **2012**, *24*, 14. [CrossRef]
3. Saleh, M.A.S. The Future Trend of E-Mobility in Terms of Battery Electric Vehicles and Their Impact on Climate Change: A Case Study Applied in Hungary. *Am. J. Clim. Change* **2024**, *13*, 83–102. [CrossRef]
4. IEA. *Global EV Outlook 2024*; IEA: Paris, France, 2024.
5. Sun, W.; Wang, B.; Wang, Z. Thermal Runaway and Thermal Management of Lithium-Ion Power Batteries in New Energy Vehicles. *Highlights Sci. Eng. Technol.* **2024**, *112*, 152–159. [CrossRef]
6. Casey, N. Fire incident data for Australian road tunnels. *Fire Saf. J.* **2019**, *111*, 102909. [CrossRef]
7. Bai, J.; Liao, H.; Xia, Y. Study on Fire Accidents in Tunnels. *IOP Conf. Ser. Mater. Sci. Eng.* **2020**, *741*, 012095. [CrossRef]
8. Li, A.; Abpeikar, S.; Wang, M.; Frankcombe, T.; Ghodrat, M. An integration framework based on deep learning and CFD for early detection of lithium-ion battery thermal runaway. *Appl. Therm. Eng.* **2025**, *274*, 126460. [CrossRef]
9. Held, M.; Tuchschmid, M.; Zennegg, M.; Figi, R.; Schreiner, C.; Mellert, L.D.; Welte, U.; Kompatscher, M.; Hermann, M.; Nachef, L. Thermal runaway and fire of electric vehicle lithium-ion battery and contamination of infrastructure facility. *Renew. Sustain. Energy Rev.* **2022**, *165*, 112474. [CrossRef]
10. Ministry of Infrastructure and Transport of the Italian Government Direttiva CE numero 2004/54/CE del 29/04/2004 | Ministero delle Infrastrutture e dei Trasporti, MIT.gov. Available online: https://www.mit.gov.it/normativa/direttiva-ce-numero-200454ce-del-29042004 (accessed on 25 March 2025).

11. McGrattan, K.B. *Fire Dynamics Simulator (Version 4): Technical Reference Guide*; National Institute of Standards and Technology: Gaithersburg, MD, USA, 2006. [CrossRef]
12. Codescu, S.; Chisacof, A.; Anghel, I.; Panaitescu, V. Environmental Consequences and Risk Factors After a Fire in a Road Tunnel. *Politeh. Univ. Buchar.* **2014**, *2*, 37–43.
13. Mazzini, V. Progetto Della Sicurezza Analisi Di Rischio. Soc. Autostrada Tirrenica PA 2015, 64. Available online: https://www.tirrenica.it/sites/default/files/2022-04/PE_DS_GN00_00_AR_001_B.pdf (accessed on 28 March 2025).
14. Autodesk Autodesk Revit. Funzionalità del Software Revit. Available online: https://www.autodesk.com/it/products/revit/features (accessed on 25 January 2025).
15. Material Properties | Website about Elements and Materials, Material Properties. Available online: https://material-properties.org/ (accessed on 28 March 2025).
16. The Engineering Toolbox Solids—Specific Heats. Available online: https://www.engineeringtoolbox.com/specific-heat-solids-d_154.html (accessed on 28 March 2025).
17. Point Veterinaire Italie. Emissivity Table. Available online: https://www.pointvet.it/web/media/libri_pvi/Tab_emissivita.pdf (accessed on 18 September 2013).
18. Camion Elettrici: La soluzione Scania, Scania Italia. Available online: https://www.scania.com/it/it/home/soluzioni-elettriche-scania.html (accessed on 15 January 2025).
19. IVECO Group. IVECO Stralis AS260S43Y/PT. 10/03. Available online: https://www.google.com/url?sa=t&source=web&rct=j&opi=89978449&url=https://www.iveco.com/altra-it/Documents/Configurator/Brochure/Stralis_IT.pdf&ved=2ahUKEwidcztveWOAxXxi_0HHc6rMVsQFnoECBUQAQ&usg=AOvVaw15qI9Rx1xJoFOH0X3U-92b (accessed on 18 February 2025).
20. SCANIA. Life Cycle Assessment of Distribution Vehicles Battery Electric vs. Diesel Driven. 6 May 2021. Available online: https://www.scania.com/content/dam/group/press-and-media/press-releases/documents/Scania-Life-cycle-assessment-of-distribution-vehicles.pdf (accessed on 17 February 2025).
21. Bhutada, G. The Key Minerals in an EV Battery, Elements by Visual Capitalist. Available online: https://elements.visualcapitalist.com/the-key-minerals-in-an-ev-battery/ (accessed on 13 January 2025).
22. The Engineering Toolbox. Metals—Specific Heats. Available online: https://www.engineeringtoolbox.com/specific-heat-metals-d_152.html (accessed on 28 March 2025).
23. Raza, H.; Li, S. The impact of battery electric bus fire on road tunnel. In *Expanding Underground—Knowledge and Passion to Make a Positive Impact on the World*, 1st ed.; CRC Press: London, UK, 2023; pp. 3280–3288. [CrossRef]
24. Lecocq, A.; Bertana, M.; Truchot, B.; Marlair, G. Comparison of the fire consequences of an electric vehicle and an internal combustion engine vehicle. In Proceedings of the International Conference on Fires in Vehicles—FIVE 2012, Chicago, IL, USA, 27–28 September 2012; pp. 183–194.
25. NFPA NFPA 502, Standard for Road Tunnels, Bridges, and Other Limited Access Highways (2020). Available online: https://www.nfpa.org/product/nfpa-502-standard/p0502code/nfpa-502-standard-for-road-tunnels-bridges-and-other-limited-access-highways-2020/50220pdf (accessed on 15 January 2025).
26. Lönnermark, E.A.; Ingason, H. *Proceedings from the Third International Symposium on Tunnel Safety and Security*; SP Sveriges Provnings-Och Forskningsinstitut: Borås, Sweden, 2008.
27. Wang, Z.; Zhu, K.; Hu, J.; Wang, J. Study on the fire risk associated with a failure of large-scale commercial $LiFePO_4$/graphite and $LiNi_x\ Co_y\ Mn_{1-x-y}\ O_2$ /graphite batteries. *Energy Sci. Eng.* **2019**, *7*, 411–419. [CrossRef]
28. Cheong, M.K.; Spearpoint, M.J.; Fleischmann, C.M. Design fires for vehicles in road tunnels. In Proceedings of the 7th International Conference on Performance-Based Codes and Fire Safety Design Methods, Auckland, New Zealand, 16–18 April 2008; pp. 229–240.
29. Verification and Validation of Selected Fire Models for Nuclear Power Plant Applications: Fire Dyna, NRC Web. Available online: https://www.nrc.gov/reading-rm/doc-collections/nuregs/staff/sr1824/v7/index.html (accessed on 15 January 2025).
30. McGrattan, K.B.; Forney, G.P. *Fire Dynamics Simulator (Version 4): User's Guide*; National Institute of Standards and Technology: Gaithersburg, MD, USA, 2004. [CrossRef]
31. Caliendo, C.; Genovese, G.; Russo, I. Risk Analysis of Road Tunnels: A Computational Fluid Dynamic Model for Assessing the Effects of Natural Ventilation. *Appl. Sci.* **2020**, *11*, 32. [CrossRef]
32. Shen, H.; Wang, H.; Li, M.; Li, C.; Zhang, Y.; Li, Y.; Yang, X.; Feng, X.; Ouyang, M. Thermal Runaway Characteristics and Gas Composition Analysis of Lithium-Ion Batteries with Different LFP and NCM Cathode Materials under Inert Atmosphere. *Electronics* **2023**, *12*, 1603. [CrossRef]
33. Betiha, M.A.; Rabie, A.M.; Ahmed, H.S.; Abdelrahman, A.A.; El-Shahat, M.F. Oxidative desulfurization using graphene and its composites for fuel containing thiophene and its derivatives: An update review. *Egypt. J. Pet.* **2018**, *27*, 715–730. [CrossRef]
34. Date, A.W. *Analytic Combustion: With Thermodynamics, Chemical Kinetics and Mass Transfer*; Cambridge University Press: Cambridge, UK, 2011.
35. Fuels—Higher and Lower Calorific Values. The Engineering Toolbox. Available online: https://www.engineeringtoolbox.com/fuels-higher-calorific-values-d_169.html (accessed on 13 January 2025).

36. Sturm, P.; Fößleitner, P.; Fruhwirt, D.; Galler, R.; Wenighofer, R.; Heindl, S.F.; Krausbar, S.; Heger, O. Fire tests with lithium-ion battery electric vehicles in road tunnels. *Fire Saf. J.* **2022**, *134*, 103695. [CrossRef]
37. BMW Group. BMW Group Vehicle Footprint—BMW i5 eDrive40, 8 May 2024. Available online: https://www.google.com/url?sa=t&source=web&rct=j&opi=89978449&url=https://www.bmwgroup.com/content/dam/grpw/websites/bmwgroup_com/responsibility/downloads/en/2025/BMW_Vehicle_Footprint_i5_eDrive40_EN_31FK.pdf&ved=2ahUKEwjFhbvTvuWOAxV7lf0HHfl3El8QFnoECBkQAQ&usg=AOvVaw354-3d0vrcjNTzChKy6Tdn (accessed on 17 February 2025).
38. Toyota. Specifiche Tecniche del Nuovo Toyota bZ4X | Toyota, Toyota IT. Available online: https://www.toyota.it/gamma/bz4x/specifiche-tecniche (accessed on 13 January 2025).
39. National Fire Protection Association; Society of Fire Protection Engineers. *SFPE Handbook of Fire Protection Engineering*, 3rd ed.; National Fire Protection Association: Quincy, MA, USA, 2022; Society of Fire Protection Engineers: Bethesda, MD, USA, 2022.
40. Wang, K.; Hu, J.; Chen, R.; Wang, J. A Study on the Evacuation of an Extra-Long Highway Tunnel Fire—A Case Study of Chengkai Tunnel. *Sustainability* **2023**, *15*, 4865. [CrossRef]
41. Idelchik, I.E. *Flow Resistance: A Design Guide for Engineers*; Routledge: New York, NY, USA, 2017. [CrossRef]
42. EdilNamAdmin. Stima Analitica Curva RHR—Approfondimento Antincendio. Available online: https://www.edilizianamirial.it/stima-analitica-curva-rhr/ (accessed on 13 January 2025).
43. Kang, S.; Kwon, M.; Yoon Choi, J.; Choi, S. Full-scale fire testing of battery electric vehicles. *Appl. Energy* **2023**, *332*, 120497. [CrossRef]
44. Aironn. Tunnel Fans. Available online: https://www.aironn.com.tr/en/products/jet-fans/tunnel-fans (accessed on 13 January 2025).
45. Li, D.; Zhu, G.; Zhu, H.; Yu, Z.; Gao, Y.; Jiang, X. Flame spread and smoke temperature of full-scale fire test of car fire. *Case Stud. Therm. Eng.* **2017**, *10*, 315–324. [CrossRef]
46. Jiang, X.; Zhu, G.; Zhu, H.; Li, D. Full-scale Experimental Study of Fire Spread Behavior of Cars. *Procedia Eng.* **2018**, *211*, 297–305. [CrossRef]
47. Okamoto, K.; Watanabe, N.; Hagimoto, Y.; Chigira, T.; Masano, R.; Miura, H.; Ochiai, S.; Satoh, H.; Tamura, Y.; Hayano, K.; et al. Burning behavior of sedan passenger cars. *Fire Saf. J.* **2009**, *44*, 301–310. [CrossRef]
48. Cui, Y.; Liu, J.; Cong, B.; Han, X.; Yin, S. Characterization and assessment of fire evolution process of electric vehicles placed in parallel. *Process Saf. Environ. Prot.* **2022**, *166*, 524–534. [CrossRef]
49. AITES. Structural Fire Protection for Road Tunnels. Available online: https://about.ita-aites.org/publications/wg-publications/1512/structural-fire-protection-for-road-tunnels (accessed on 16 July 2025).
50. PIARC. Impact on Outside Air Quality | Road Tunnels Manual—World Road Association (PIARC). Available online: https://tunnelsmanual.piarc.org/en/operation-and-maintenance-environmental-issues/impact-outside-air-quality (accessed on 15 January 2025).